

Biocompatible Semiconductor Quantum Dots as Cancer Imaging Agents

Kevin J. McHugh, Lihong Jing, Adam M. Behrens, Surangi Jayawardena, Wen Tang, Mingyuan Gao, Robert Langer,* and Ana Jaklenec*

Approximately 1.7 million new cases of cancer will be diagnosed this year in the United States leading to 600 000 deaths. Patient survival rates are highly correlated with the stage of cancer diagnosis, with localized and regional remission rates that are much higher than for metastatic cancer. The current standard of care for many solid tumors includes imaging and biopsy with histological assessment. In many cases, after tomographical imaging modalities have identified abnormal morphology consistent with cancer, surgery is performed to remove the primary tumor and evaluate the surrounding lymph nodes. Accurate identification of tumor margins and staging are critical for selecting optimal treatments to minimize recurrence. Visible, fluorescent, and radiolabeled small molecules have been used as contrast agents to improve detection during real-time intraoperative imaging. Unfortunately, current dyes lack the tissue specificity, stability, and signal penetration needed for optimal performance. Quantum dots (QDs) represent an exciting class of fluorescent probes for optical imaging with tunable optical properties, high stability, and the ability to target tumors or lymph nodes based on surface functionalization. Here, state-of-the-art biocompatible QDs are compared with current Food and Drug Administration approved fluorophores used in cancer imaging and a perspective on the pathway to clinical translation is provided.

1. Introduction

Cancer is the leading cause of death worldwide and incidence is only expected to increase further due to an aging population and mounting environmental risk factors.^[1] In the United States alone, 600 000 people die each year from cancer and 1.7 million new cases are diagnosed.^[2] While some cancers have relatively high five-year survival rates if diagnosed when

cancer cells remain localized at the primary tumor site and sentinel lymph nodes (SLNs), prognosis is poor for solid tumors that are not discovered before becoming metastatic.^[2] Therefore, there has been a major emphasis on early screening with the goal of detecting the disease at a stage when it is easier to treat, which is especially important for cancers that are aggressive or asymptomatic in their early forms.^[3]


Cancer diagnosis often relies on a combination of biopsy and imaging, which can consist of X-ray computed tomography (CT), magnetic resonance imaging (MRI), positron emission tomography (PET), single photon emission CT (SPECT), ultrasound, and optical imaging. Tomographical techniques (CT, MRI, PET, and SPECT) provide morphological data that helps to identify structural abnormalities consistent with tumors and have no practical imaging depth limitations, but can be limited by resolution and contrast if cancerous tissue is sufficiently similar to healthy tissue.^[4–6] In addition, these

modalities require large, expensive equipment and long image collection times which precludes their use during surgical procedures. Real-time imaging of tumors during surgery is important to ensure that the tumor be completely excised and thus prevent recurrence while avoiding unnecessary tissue removal that would contribute to morbidity and loss-of-function. Intraoperative imaging can also be helpful for the collection of biopsy specimens for the clinical staging of cancer. For some cancers, including certain forms of breast cancer, the standard of care is SLN biopsy concurrent with surgical resection of the primary tumor. The data obtained from the histological analysis of these samples can serve to inform doctors about the spread of the disease and best course of treatment.

Radiolabeled and fluorescent small molecules have been the most commonly agents used to identify lymph nodes that drain from the tumor site. Radiolabeling offers the advantage of high sensitivity, but shows little specificity for tumor or lymphatic tissue leading to a poor signal-to-noise ratio between normal tissue and the tissues of interest. In addition, radiolabeled compounds (typically technetium-99m)^[7] also have an added health concern associated with radiation. Fluorescence imaging offers high sensitivity, excellent resolution (1 μm) at the tissue

Dr. K. J. McHugh, Dr. L. H. Jing, Dr. A. M. Behrens, Dr. S. Jayawardena, Dr. W. Tang, Dr. R. Langer, Dr. A. Jaklenec
David H. Koch Institute for Integrative Cancer Research
Massachusetts Institute of Technology
77 Massachusetts Avenue, Cambridge, MA 02139, USA
E-mail: rlanger@mit.edu; jaklenec@mit.edu

Dr. L. H. Jing, Dr. M. Y. Gao
Institute of Chemistry
Chinese Academy of Sciences
Bei Yi Jie 2, Zhong Guan Cun, Beijing 100190, China

 The ORCID identification number(s) for the author(s) of this article can be found under <https://doi.org/10.1002/adma.201706356>.

DOI: 10.1002/adma.201706356

surface, and requires relatively inexpensive equipment, but is limited by the suboptimal properties of fluorophores currently approved by the United States Food and Drug Administration (FDA) for cancer indications such as nonspecific tissue distribution, lack of stability, rapid clearance, and excitation and emission at wavelengths that do not pass through tissue well. Although there is an inherent reduction in the spatial resolution of fluorescence imaging with imaging depth due to light absorption, scattering, and tissue autofluorescence, these issues can be mitigated, in part, by selecting fluorescent materials with specific emission spectra that pass more readily through biological tissues.

The three fluorescent dyes currently approved by the FDA for cancer imaging are 5-aminolevulinic acid (5-ALA, fluorescence-guided surgery), methylene blue (SLN mapping), and indocyanine green (intraoperative tumor identification).^[8–10] 5-ALA is approved for fluorescence-guided surgery, but is excited and emits at wavelengths (405/645 nm) that are heavily absorbed by tissue, which severely hinders imaging depth. Methylene blue is approved for SLN mapping and has more appropriate excitation and emission peaks (668/688 nm), but cannot be used at high doses due to the potential for toxic metabolic encephalopathy, is cleared quickly from tissue, and exhibits a small Stokes shift with largely overlapping spectra, making it difficult to differentiate between reflected excitation light and emitted light.^[11–14] As a result, methylene blue is typically used for its visibly intense blue color and not for fluorescence imaging. Indocyanine green also has fairly favorable excitation and emission peaks (807/822 nm), but has poor thermal and photostability, a small Stokes shift, and low photoluminescence quantum yield (PL QY) leading to low imaging contrast.^[13,14] In addition, because all three are small molecule dyes, they are cleared quickly by the lymph system.^[15–19] Overall, however, the lack of penetration depth is likely the main reason that fluorescence imaging is not more prevalent in the clinic despite its expanded use in small animal preclinical studies where the required depth of penetration is often <1 cm.^[20] Therefore, the development of probes that overcome the challenges associated with signal intensity, stability, and tissue penetration will be essential for more extensive clinical implementation.

Colloidal quantum dots (QDs) are an appealing platform for optical cancer imaging because of their tunable and unique optical properties compared to organic small molecule dyes (Table 1). QDs can be synthesized with favorable fluorescent properties including a large Stokes shift, long fluorescence lifetime, narrow emission band, and most importantly, NIR emission (650–950 and 1000–1350 nm) to maintain high resolution for deeper imaging, which make them suitable as direct substitutes for existing dyes. In addition, they can also be designed to achieve superior tumor targeting and improved retention time, can act as probes for multiple imaging modalities, and have the potential to provide nonmorphological data.^[13,21–27] As a result, QDs have the potential to not only replace existing dyes for SLN mapping and intraoperative surgery, but also to provide opportunities for tumor characterization and potentially deeper imaging. Here, we focus on the use of biocompatible (i.e., heavy metal-free) QDs for cancer imaging. We aim to review the field as a whole, highlight promising work, and discuss the future steps needed to translate



Kevin McHugh is a Ruth L. Kirschstein Postdoctoral Fellow in Dr. Robert Langer's laboratory at the Massachusetts Institute of Technology (MIT). Prior to working at MIT, he received his B.S. in biomedical engineering from Case Western Reserve University in 2009 and Ph.D. in biomedical engineering from Boston



University in 2014. His current research focuses on the development of microfabricated polymer systems for the controlled delivery of therapeutics and diagnostic agents.

Robert Langer is one of 13 Institute Professors (MIT's highest honor). He grew up in Albany, New York, attending the public schools there. He then went to Cornell University where he received a B.S. in chemical engineering and MIT where he received an Sc.D. in the same field. He then did postdoctoral work at Boston's children's hospital before joining the MIT faculty in 1977. His research interests are in drug-delivery systems, biomaterials, nanotechnology, tissue engineering, and regenerative medicine.



Ana Jaklenec is a Research Scientist at Massachusetts Institute of Technology in the laboratory of Robert Langer at the David H Koch Institute for Integrative Cancer Research. Her group is focused on controlled delivery and stability of cell, biologic and small molecule therapeutics and has a strong focus on technologies for developing world applications. Dr. Jaklenec holds a B.S. in biomedical engineering from Boston University and a Ph.D. in biomedical engineering from Brown University.

this technology to the clinic. In particular, copper and silver chalcogenide I–VI and I–III–VI QDs have been emphasized due to their prevalence and favorable in vivo properties. These QDs represent some of the most promising heavy metal-free compositions for in vivo applications because their excitation and emission ranges from the visible to the NIR and because

Table 1. Advantages of QDs as fluorescent imaging probes.

Optical properties	Functional outcomes
Tunable emission into the NIR	Enables deeper tissue imaging (possibly >2 cm when emission is in the NIR II biological imaging window) due to a two log-order reduction in tissue absorbance ^[28]
Broad excitation range, narrow emission, and a large Stokes shift	Enables simultaneous multiplexed imaging with a single excitation source
High photoluminescence quantum yield	High imaging contrast
Long photoluminescence lifetime	Enables time-gate detection for reducing autofluorescence
Stable (resistant to photobleaching and other environmental factors)	Allows for long-term exposure
Compatible with biomolecular functionalization and the EPR effect	Capable of targeting a tumor or lymphatics

they exhibit fluorescence PL QY of up to 50% after proper surface passivation.

2. Semiconductor Quantum Dots

Colloidal QDs, also known as semiconductor nanocrystals, are nanoparticles composed of elements from Groups II–VI, II–V, III–V, IV–VI, I–VI, I–III–VI, IV, or that exhibit unique optical properties governed by the quantum confinement effect. These properties arise from particle size, which is on the order of, or smaller than, the exciton Bohr radius of the corresponding bulk material. Particles are synthesized using an inexpensive and scalable liquid phase technique that can be tuned to achieve different fluorescent properties by altering elemental composition and size. With very few exceptions, QDs are synthesized with wide band gap semiconductor shells that improve optical properties. QD synthesis and properties have been comprehensively reviewed by others (Zhong et al.,^[29] Dubertret and co-workers^[30] Kolny-Olesiak and Weller,^[31] Gao and Rogach,^[32] Reiss and co-workers,^[33–35] Gamelin and co-workers,^[36] Prasad and co-workers,^[37] and Ryan and co-workers^[38]) and will therefore not be explained in great detail here. However, it is important to note that for a vast majority of biomedical applications, QDs are nanoparticles with a fluorescent core, semiconductor

shell, surface functionalization that enables their dispersion in water, and functionalized with other biomolecules to target specific proteins expressed on the surface of the cells of interest (**Figure 1**). QD research has largely focused on materials from Group II–VI such as cadmium, lead, and mercury for the core materials; however, many of these elements are known to exhibit substantial toxicity in the body, even at low levels. Bawendi has been a pioneer of the advancement of heavy metal free-quantum dots, first reporting the fabrication of Group I–III–VI QDs via a hot-injection method,^[39] which are very promising for in vivo applications because they can be excited by incident light and emit at >600 nm. As a result, over the past ten years many researchers interested in using QDs for biomedical applications have shifted toward synthesizing heavy metal-free compositions from Groups I–VI and I–III–VI containing elements such as Cu, Ag, In, Zn, S, and Se to improve biocompatibility.

2.1. Advantages of Imaging with Quantum Dots

QDs present an excellent alternative to traditional organic fluorophores because their size, surface chemistry, spectral properties, and stability can be easily tuned to optimize in vivo imaging. By altering composition or size, many groups have been able to create QDs with a wide variety of emission wavelengths, high absorption coefficients, and large Stokes shifts (180–500 meV), while exhibiting significantly reduced toxicity relative to QDs containing heavy metals.^[29,34,40–47] In general, the most important optical characteristics for biomedical imaging applications are the: (1) broad excitation, (2) tunable fluorescence ranging from the UV-blue to the mid-IR and narrow full-width at half-maximum (FWHM) of the PL profile, (3) high PL QY, (4) long PL lifetime, and (5) long-term photostability. The emission window and FWHM can be tuned by altering the size, size distribution, composition, and crystal structure of QDs. This is especially true for ternary QDs, which can accommodate substantial off-stoichiometry deviations. To date, I–VI and I–III–VI QDs with fluorescent emission peaks that span from the visible range to the near-infrared (NIR) have been synthesized by altering elemental composition and size. QDs with emission in the visible range are largely limited to in vitro biomedical applications due to the high level of visible absorbance by tissue, as shown in **Figure 2**. Alternatively, NIR

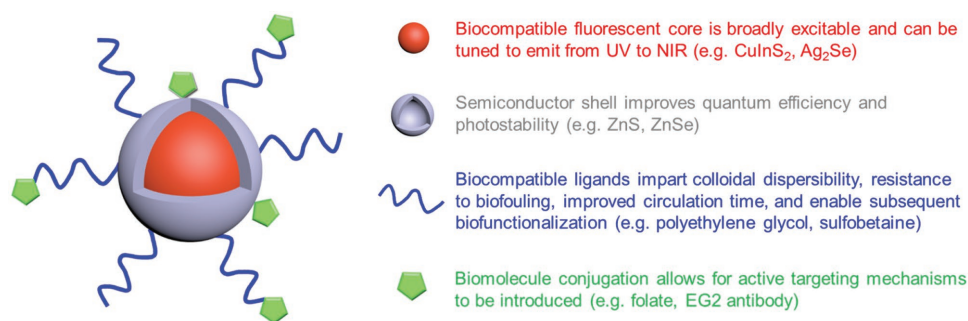


Figure 1. Schematic of a typical quantum dot structure containing a fluorescent core, wide bandgap semiconductor shell for surface passivation, and surface ligands that enable dispersion in water and molecular targeting.

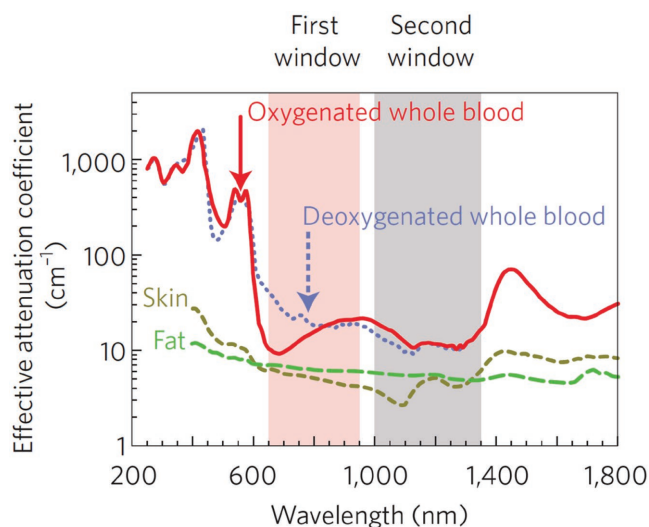


Figure 2. Graph depicting the NIR I (650–950 nm) and NIR II (1000–1350 nm) biological imaging windows corresponding to reduced absorption by skin, fat, and blood. Aggregate absorption is generally lowest in the NIR II window depicted in gray. Reproduced with permission.^[28] Copyright 2009, Macmillan Publishers Ltd.

light passes more readily through biological tissue with lower absorption and scattering, which enables QDs in the NIR range to maintain their high resolution even when imaging deeper tissues *in vivo*.^[9,10,28,48–51] As a result, the majority of work developing emission-tunable QDs as *in vivo* imaging probes has been focused on heavy-metal free QDs that excite and emit strongly in the NIR, which substantially increases contrast, sensitivity, and penetration depth while avoiding optical damage to the body. Ultimately, NIR I-emitting fluorophores will be limited to imaging structures less than 2 cm in depth due to signal attenuation from tissue scattering.^[28,52] For indocyanine green, the FDA-approved fluorophore with the best spectral properties, imaging was found to be difficult even at a depth of 1 cm due to poor tissue penetration.^[53] Short-wave infrared light (1000–2000 nm) passes even more readily through biological tissue, but is inefficiently detected by traditional CCD cameras and will require the adoption of InGaAs detectors for optimal signal collection.^[28,54] However, using InGaAs detectors in combination with NIR II-emitting QDs with high PL QY can potentially enable greater imaging depths (>2 cm) than can be achieved by conventional small molecule dyes in the NIR II range that suffer from low PL QY and poor stability.^[51,55–60]

Epitaxial growth of a wide band gap semiconductor shell on top of the QD core has been a common approach for improving the fluorescent properties of QDs since the 1990s.^[61–64] Coating QDs with a shell composed of a material such as ZnS (≈ 3.61 eV) can enhance photostability and PL QY by removing surface trap states and confining the photoexcited charge carrier.^[32–34,42,43,46,65–70] The small intrinsic lattice mismatch between the I–III–VI core and ZnS shell allows the shell to readily undergo epitaxial growth, which can enhance fluorescence PL QY to >50% and improve photostability. In addition, adding a shell generally increases the average lifetime of the fluorescence decay process up to several hundreds of

nanoseconds since the fast decay channels associated with trap states are eliminated. These long fluorescence lifetimes compared to indocyanine green (0.166 ns),^[71] for example, allow for time-gated imaging, which can reduce background fluorescence and thereby improve the signal-to-noise ratio (i.e., contrast).^[43] Shell overgrowth on I–III–VI QDs can also be used to shift the emission wavelength as Zn competes with the shell epitaxial growth process.^[40,43,68,69,72] This feature is especially useful for bioimaging because it enables researchers to precisely tune the emission peak of QDs for optimal tissue penetration by forming quaternary QDs such as Cu–In–Zn–S or Cu–In–Zn–Se QDs.^[33,73,74]

Unlike traditional organic dyes, QDs also have the potential to be used as multiplexed imaging probes. While current FDA-approved dyes emit broadly on the order of hundreds of nanometers, QDs can have emission line widths as narrow as 20–50 nm (<100 meV).^[75,76] As a result, multiple QD populations targeting different molecules or tissues can be used to simultaneously visualize a variety of cancer-related biomarkers or events using a single excitation source. Because the narrowest emission bands have traditionally been associated with toxic II–VI Cd(Se,Te) QDs, significant effort has recently focused on the production of biocompatible ternary I–III–VI chalcogenide QDs such as Cu–In–S and Cu–In–Se, which normally have emission widths on the order of 80–150 nm due to the presence of multiple recombination channels.^[29,35,36,42,43,68] Klimov and co-workers recently demonstrated the ability to narrow the PL emission width of a single dot down to 60 meV (≈ 20 nm) through epitaxial coating of the CuInS₂ core with a relatively thick (up to six layers) ZnS shell, which was thought to reduce the positioning heterogeneity of Cu defect-related emission centers in the encapsulated QD.^[46] Therefore, narrow emission line widths can be achieved even with biocompatible compositions and potentially enable the simultaneous use of dozens of probes spread across the NIR I and NIR II windows at a single time for advanced cancer characterization. For example, QDs with different emission peaks functionalized with specific surface molecules could be used to detect various aspects of the tumor microenvironment including heterogeneous upregulation of surface proteins,^[77] enzymatic activity,^[78] and pH.^[79]

2.2. Water-Dispersible Quantum Dots

To be useful for most biomedical applications, QDs must be capable of forming a dispersion under physiological conditions (aqueous, pH 7.4, 37 °C, and in the presence of salts, proteins, and other biological molecules). This can be achieved spontaneously during aqueous phase synthesis or using a secondary surface modification process after organic phase synthesis. One common strategy used to enable QD dispersion in water is ligand exchange, which replaces hydrophobic ligands with hydrophilic counterparts and does not substantially impact the hydrodynamic diameter of QDs as long as the substituted ligand is small. To improve the stability of QDs after ligand exchange, ligands with strong affinity for binding metal ions, often containing thiol groups, are used. However, low pH can cause the dissociation or oxidation of monodentate thiols.^[80]

To avoid this dissociation issue, ligands containing a hydrophobic spacer between the thiol and the hydrophilic group have been utilized to create QD dispersions that are stable for over a month.^[81] Another strategy to generate homogeneous dispersions under aqueous conditions after organic phase synthesis is to encapsulate the QDs in an amphiphilic polymer. The hydrophobic portion of the amphiphile interacts with the hydrophobic ligands on the QD surface, while the hydrophilic end provides repulsion between QDs. The advantages of amphiphilic encapsulation include improved stability in comparison with the monodentate ligand-capped QDs and the capacity to provide abundant functional groups for further chemical modification.

Although the majority of I–VI and I–III–VI QDs have been produced using organic phase synthesis, aqueous phase synthesis is attractive because it is environmentally friendly and eliminates the phase-transferring process, which reduces production time and cost.^[32,82] Once QDs can be dispersed in water, they can be used directly to target tumors via the enhanced permeation and retention (EPR) effect or be functionalized with peptides, proteins, and nucleic acids to further improve tumor targeting.^[83,84]

2.3. Exploiting the EPR Effect

Water dispersible QDs have been shown to passively accumulate at the site of a tumor, which has largely been attributed to the EPR effect. The EPR effect arises from pathologies that cause increased vascular permeability, as is the case with solid tumors, in which poorly (and often rapidly) produced blood vessels do not form a tight transport barrier. Increased vascular permeability allows for nanoparticle systems to extravasate through the capillary wall and accumulate into pathological tissue while being excluded from healthy tissue. The typical size range of QDs (<100 nm) makes them extremely well suited for taking advantage of cancer-related vascular fenestrations.^[85]

The accumulation of particles in cancerous tissue by the EPR effect can be further improved by increasing particle circulation time, which is generally accomplished by reducing particle uptake by the reticuloendothelial system (RES). The most common approach to increasing circulation time of QDs and other nanoparticles is through surface modification with polyethylene glycol (PEG). This strategy has been widely applied to QDs in the form of covalent surface modifications or by incorporating PEG into micelles. Limitations of PEG modification, including the induction of PEG-resistant macrophages that reduce QD circulation time, have led to alternative functionalization approaches with equivalent aims. Surface-modifying zwitterionic ligands can also be used to improve circulation time while providing an opportunity for performing additional modifications through the presence of multiple functional groups. While exploiting the EPR effect represents a simple mechanism for localizing QDs by passively taking advantage of solid tumor physiology, its only moderate selectivity for tumors will likely limit the utility of therapies and diagnostics that exclusively rely on this effect. Therefore, more recent studies have aimed to incorporate active targeting moieties that further improve selectivity for cancerous tissue compared to healthy tissue.

2.4. Surface Modification for Cancer Targeting

The incorporation of active targeting moieties onto QD surfaces has been the most common approach used to improve tumor site accumulation and preferential cancer cell-specific interactions. This strategy aims to take advantage of upregulated receptors or other surface proteins that can be directly targeted via ligand–receptor interactions or antibodies. Nanoparticles functionalized with folic acid are frequently reported because folate receptors are overexpressed in a variety of human tumors, but are minimally expressed by healthy cells. Even after folic acid is conjugated to the nanoparticle surface, the nanoprobe remains small and can therefore continue to benefit from the EPR effect. However, the conjugation reaction between folic acid and nanoparticles typically has to be carried out in a mixture of water and organic solvent due to the poor water solubility of folic acid, and then the conjugates need to be further transferred into aqueous media. This challenge was recently overcome through modification of folic acid via covalent coupling with two Jeffamine polyetheramines. This resulting modified folic acid is highly water soluble and favors a coupling reaction with nanoparticles in the aqueous phase through the remaining amino group on Jeffamine.^[86]

QD targeting based on the overexpression of cell surface proteins has been reported for breast and pancreatic cancer. Liu et al. published a CuInSe₂/ZnS based core–shell system surface conjugated with Cys–Gly–Lys–Arg–Lys (CGKRRK), a peptide that binds to a tumor cell membrane biomarker.^[81] They used this system to target mice bearing an orthotopic MCF10CA1a breast cancer xenograft. Yong et al. used CuInS₂/ZnS QDs encapsulated in folic acid functionalized PEGylated phospholipid micelles to target overexpressed folic acid receptors in pancreatic cancer cells (Panc-1) in nude mice.^[87] Yu et al. describes using CuInS₂/ZnS core–shell QDs for in vivo imaging of a U87MB brain tumor in mice.^[88] The QD system is bioconjugated to the antibody EG2, which binds to epidermal growth factor receptor (EGFR)—a protein commonly upregulated in cancer. This surface moiety improved tumor targeting resulting in higher fluorescence intensity at the tumor site relative to QDs that were not modified with EG2. However, the discovery of more specific tumor targets will be critical for improving tumor targeting since implementation is currently limited by the ability to identify proteins that are vastly overexpressed as well as the potential immunogenicity of targeting moieties and possible negative impacts of conjugation on other QD properties.

3. Biocompatibility

The biocompatibility of QDs is largely dependent on their elemental composition, surface properties, and size, which can affect the mechanisms of toxicity involved as well as biodistribution and clearance.

3.1. Quantum Dot Toxicity

The toxicity of first generation Cd-based QDs has, for the most part, eliminated the potential for their use in human patients

due to the high cytotoxicity of Cd^{2+} , which can be released from QDs after administration.^[89–93] Depending on the stability and clearance of the QDs used, degradation-associated toxicity may occur immediately or later during the chronic stage of the foreign body reaction as QDs disintegrate and release metal ions into the body. Although this potential mechanism of toxicity applies to all QDs, regardless of their composition, it is particularly problematic for Cd-based ones due to the high cytotoxicity of Cd^{2+} , which causes oxidative stress, affects protein binding, and stimulates inflammatory cytokine production.^[89,90,94] In order to mitigate this, early efforts employed a ZnS coating to prevent Cd^{2+} release. While these ZnS-coated Cd QDs were much less toxic than identical uncoated QDs in vitro, they degraded in the low pH of the rat digestive tract indicating the continued possibility of Cd^{2+} release and thus in vivo toxicity.^[95,96] A recent meta-analysis of Cd-based QD toxicity has been carried out by Medintz and co-workers using a random forest regression model to analyze 1741 cell viability-related data from 307 publications.^[97] The results from this study show that cellular toxicity of Cd-based QDs is primarily determined by their intrinsic properties (size, surface ligand, shell, and surface modification), which may be representative of other QD core compositions as well, though more analysis is needed. As a result, recent research has focused on QDs composed of more well-tolerated elements functionalized with coatings that allow them to be readily cleared from the body.

To avoid heavy metal-associated toxicity, many researchers have turned to Cu- and Ag-based QDs, which have shown markedly lower toxicity compared with Cd-based QDs both in vitro and in vivo.^[68,72,98–100] For example, PEGylated $\text{CuInS}_2@ \text{ZnS:Mn}$ QDs functionalized with a dihydropolipoic acid-poly(ethylene glycol) (DHLP-PEG) ligand only became cytotoxic in HeLa cells at 7000-fold the cytotoxic dose level for CdTe QDs, (half maximal inhibitory concentration of $\approx 167.9 \mu\text{mol L}^{-1}$ compared to $\approx 0.023 \mu\text{mol L}^{-1}$).^[68] This nearly four-log improvement in cytocompatibility has driven the rapid development of heavy metal-free QDs, such as those included in **Table 2**, and improved formulations are constantly emerging.^[19,34,37,101]

Wang and co-workers showed that a 30 mg kg^{-1} injection of PEGylated- Ag_2S QDs did not affect body weight over the course of two months in a mouse model and only caused a small drop in platelet and white blood cell counts in the first few days after injection.^[99] Another study showed that 100 pmol of $\text{CuInS}_2/\text{ZnS}$ QDs produced the same degree of axillary lymph node inflammation in mice as 10 pmol of $\text{CdTeSe}/\text{CdZnS}$ —a tenfold

improvement.^[72] Despite this exploratory work, there is still a distinct lack of long-term systematic investigations on toxicology and pharmacokinetics for QDs. Other strategies such as secondary encapsulation in biocompatible materials may also assist in improving colloidal stability and thereby prevent leakage from the core into the internal milieu.^[94,136] The in vivo toxicity of Cd-free QDs has been well summarized in a recent review.^[37]

In addition to elemental toxicity based on QD composition, there are several mechanisms that may contribute to toxicity including the light-dependent production of reactive oxidative species that are broadly damaging to cells,^[137] translocation into nucleus resulting in DNA damage,^[1,138,139] and deleterious physical interactions with cell components, such as the mitochondria.^[140,141] Because these mechanisms will continue to induce a negative biological response for the duration of their residence in tissue, it is important that QDs be readily cleared from the body once they are no longer needed as contrast agents. Even if QDs are administered locally and excised along with the tumor or sentinel lymph nodes, some may still enter the circulation leading to systemic availability and residence. Ideally QDs would be administered, accumulate in the desired tissues for an application-specific period of time (several hours to one day), avoid a significant foreign body reaction, and be readily cleared by the renal system.

3.2. Quantum Dot Clearance and Excretion

QD clearance and excretion is largely modulated by their surface properties and size. Surface properties can substantially impact QD toxicity through protein adsorption after injection. This adsorption to the surface can result in a “protein corona” in accordance with the Vroman Effect, which increases the effective hydrodynamic diameter and promotes macrophage phagocytosis by the RES.^[142,143] Therefore, many cancer applications may benefit from protein adsorption-resistant QD surfaces to promote timely clearance since toxicity issues are exacerbated by poor tissue clearance as QDs tend to accumulate in the liver, kidney, and spleen if not designed appropriately. For example, one study showed that amino-PEG-coated Cd-based QDs with hydrodynamic size of 41.2 nm were directly injected into tumor, and the fluorescence still can be detectable in the body after two years, which may be a critical issue for clinical translation.^[144] This can cause morphological alterations to the lobules

Table 2. Properties of commonly studied fluorescent colloidal I–VI and I–III–VI heavy metal-free chalcogenide quantum dots.

Composition	Bulk band gap at 300 keV	Exciton Bohr radius [nm]	Emission range ^{a)} [nm]	References
Ag_2S	0.93	2.2	510–1294	[45,102–113]
Ag_2Se	0.15	2.9	700–1300	[47,49,114–119]
Ag_2Te	0.67	–	900–1300	[115,120,121]
CuInS_2	1.53	4.1	500–950	[29,31,33,40,42,43,69,122]
CuInSe_2	1.05	10.6	650–1200	[39,123–126]
AgInS_2	1.87	5.5	535–830	[127–131]
AgInSe_2	1.20	6.4	592–1200	[41,126,129,132–135]

^{a)}Photoluminescent emission ranges of stoichiometric and off-stoichiometric compositions including core–shell structures.

of the liver, increase oxidative stress, and significantly increase levels of malondialdehyde in hepatocytes.^[88,145,146] Therefore, studying the excretion pathway and clearance kinetics of QDs may help determine the properties needed to minimize chronic tissue damage.

Size is perhaps an even more important factor in QD clearance and excretion because the kidney's filtration cut-off size is 6–8 nm. Therefore, QDs with a hydrodynamic diameter below this threshold could theoretically be cleared through renal excretion while larger QDs will likely be uptaken by the liver. One study showed that 30–99% of intravenously (IV) delivered nanoparticles larger than 6 nm in diameter were sequestered in the liver and excreted slowly in feces over days, months, or even years depending on the composition studied.^[147] In the liver, QDs first encounter Kupffer cells, which phagocytose larger nanoparticles more rapidly than smaller ones. This size effect has been demonstrated in vitro using macrophages for larger Au nanoparticles, in which 90 nm particles were more readily taken up than 30 nm particles^[148] and superparamagnetic iron oxide nanoparticles (60 nm versus 20 nm).^[149] QDs that evade phagocytosis by Kupffer cells may then pass through sinusoidal fenestrations and reach hepatocytes if they are less than 200 nm in diameter. In hepatocytes, the foreign QDs are degraded, excreted into the bile, and finally cleared through defecation. For 18.5 nm PEGylated nanoparticles, excretion was observed in feces both 3 and 14 d after IV injection.^[150] However, it would be preferred if QDs were small enough to be filtered out by the kidneys (<6 nm) and thereby minimize potentially harmful uptake by liver cells.

Rapid renal clearance has been demonstrated for zwitterionic and neutral organic-coated QDs with a final hydrodynamic radius of less than 5.5 nm.^[151] Coating QDs with zwitterionic ligands, such as cysteine, glutathione,^[152] dithiolated polyaminocarboxylate,^[153] and dopamine sulfonate^[154] have all been reported to enhance renal excretion. PEGylation is another approach for potentially reducing QD–protein interactions; however, the effect of chain length (i.e., molecular weight) on hydrodynamic radius must also be considered. Surface properties also dictate the interaction of nanoparticles with hepatocytes. For example, positively charged mesoporous silica nanoparticles were readily endocytosed by hepatocytes in vivo, while negatively charged nanoparticles were not, presumably due to rapid sequestration by Kupffer cells during first pass metabolism.^[155] The time-to-clearance, however, may be difficult to predict without empirically studying each formulation. For example, one report showed the degradation of Ag₂Se QDs into Ag⁺ and Se²⁻ within one week^[156,157] while another study showed that a different Cd-free QD, Bio CFQD, was cleared from the liver after two months^[158] and a third study showed significant retention of large QDs (29.6 nm) in the spleen and liver after one month accompanied by signs of kidney damage.^[156]

QD stability also plays an important role in function, toxicity, and clearance. As such, synthesis strategies should account for the effects of QD degradation by modulating composition and surface treatment. Chemical composition and surface ligands are two key factors that help to determine the chemical stability, fluorescence stability, and clearance of QDs in vivo. The aqueous solubility and oxidation-reduction potential of the

constituent materials used in QD cores and shells can favor dissolution or prevent degradation. Surface ligands can also prevent degradation by shielding QDs from the surrounding environment. In principle, because of the low solubility of semiconductor compounds in water, most QDs with strongly bound ligands possess high chemical stability against enzymes in macrophage lysosomes.^[136] Therefore, researchers should utilize these properties to design their QDs to remain stable for the duration of their particular imaging application.

4. Preclinical Quantum Dot Imaging in Cancer

4.1. Near-Infrared Optical Imaging

Fluorescence imaging can be categorized according to the emission wavelength of the fluorophore. The most abundant fluorescence imaging agents fall in the visible region; however, performance of fluorophores in the visible region is severely hindered by strong tissue autofluorescence, absorption, and photon scattering. Therefore, fluorescence imaging in the NIR-I (650–950 nm) and NIR-II (1000–1350 nm) regions can be used to improve signal-to-noise ratio by operating in a spectral region of low tissue autofluorescence thereby reducing photon scattering and penetrating deeper into tissues due to a reduction in cumulative absorbance by water and hemoglobin. In recent years, many heavy element-free QDs have been developed with emission in the NIR-I and NIR-II windows. Various methods have been employed to reach emissions of higher wavelength such as fine tuning the core precursor ratios,^[81,159,160] varying the core synthesis temperature to increase core size,^[123] and using the seeds of the initial growth for a secondary growth process.^[161] These NIR emitting QDs have been used in vivo for various proof-of-concept experiments to demonstrate both active and passive tumor targeting for real-time imaging of tumors as described in Table 3 including imaging of breast cancer xenografts in mice,^[146] real time SLN mapping of metastatic breast cancer in mice,^[162] and in vivo imaging of glioblastoma.^[88]

4.2. Optical Imaging in the NIR-I Region for Primary Tumor Localization

Two of the most robust QD compositions with NIR photoluminescence comparable to heavy metal-containing QDs are the ternary CuInS₂ and CuInSe₂ core–shell systems. Dubertret's group synthesized a CuInSe₂/ZnS tertiary core–shell QD system for NIR in vivo imaging with a PLQY that was 40–50% higher than without the ZnS shell.^[171] The addition of the ZnS shell contributes to the stability of the core by preventing the core from oxidation. Their QDs were then made hydrophilic by exchanging the hydrophobic ligand with a thiol containing zwitterionic sulfobetaine and used to image the right axillary lymph node of mice, after a subcutaneous injection of QDs into the right anterior paw. QDs travelled to the lymph node and were visible after few minutes and remained visible for several hours after being injected.

Liu et al. also developed NIR (709 nm) CuInSe₂/ZnS core–shell QDs that were surface conjugated with the tumor targeting peptide Cys–Gly–Lys–Arg–Lys (CGKRK) through a

Table 3. Preclinical use of biocompatible quantum dots in cancer imaging.

Imaging technique	Composition	Surface functionalization	Size	Peak emission and PL QY	Route and dose	Studies, animal model/clearance	References
NIR-I optical imaging	CuInS ₂ /ZnS	DHLA-PEG1000	≈3 nm (TEM), ≈20–22 nm (HD)	800 nm, ≈20%	SQ ^{a)} at 20 pmol per animal	SLN imaging in mice, reduced toxicity	[72]
NIR-I optical imaging	CuInS ₂ /ZnS	FA-SOC micelle	≈4 nm (TEM), ≈200 nm (HD)	800 nm, ≈20%	IV at ≈8 μg g ⁻¹ body weight	Active targeting to receptor-positive Bel-7402 tumor imaging	[163]
NIR-I optical imaging	CuInS ₂ /ZnS	DSPE-PEG-FA micelle	3–5 nm (TEM), 40–90 nm (HD)	695 nm, 35%	IV at 0.5 mg per animal	Active targeting to Panc-1 tumor visible as early as 15 min post-injection, in vivo multiplex imaging	[164]
NIR-I optical imaging	CuInS ₂ /ZnS	33% PEG2000-COOH + 66% PEG2000 lipid micelles	≈20 nm (HD)	780 nm	SQ injection of 20 pmol per animal	SLN imaging in a metastatic breast 4T1 tumor, increase of In concentration from 1 to 8 h post-injection, followed by a rapid drop of fluorescence intensity from 8 to 72 h through feces, urine	[162]
NIR-I optical imaging	CuInS ₂ /ZnS	EG2	6.6 nm (TEM)	790 nm, 8%	IV at 20 μL of 1 μm solution	Active targeting to brain U87MG. EGFRvIII glioblastoma tumor in mice, high level PL in tumor after 4 h of injection	[88]
NIR-I optical imaging	CuInSe ₂ /ZnS	CGKRK peptide	36 nm (HD)	709 nm	Intracranial micro-injection at 100 μL, 2 nmol QD g ⁻¹ body weight	Active targeting for brain glioblastoma tumor imaging in NG2 positive bearing mice, strong PL signals in the brain highlighted the tumor boundaries and even the so-called “guerilla” tumor cells that diffusely infiltrate at the invasion front	[81]
NIR-I optical imaging	Cu–In–Se/ZnS	Ligand bearing dithiol and sulfobetaine zwitterionic	2–5 nm (TEM)	800 nm, ≈20%	SQ at 20 μL (0.5 OD@ 690 nm) per animal	Regional LN imaging	[123]
NIR-I optical imaging	AgInS ₂	Pluronic F127 triblock copolymer micelle	3.5–4.5 nm (TEM), 10 nm (HD)	800 nm, 35%	IV at ≈3 mg per animal	Passive targeting of fibrosarcoma tumor through the EPR effect	[98]
NIR-I optical imaging	AgInS ₂	poly(acrylic acid)-graft-mercaptoethylamine (PAA-g-MEA)	6.3 nm (TEM), 8.5 nm (HD)	817 nm, 34.4%	SQ at 2 μg per animal, Tail vein IV at 10 μg per animal	Whole body imaging, high PL for 12 h P.I. (sub), High PL for 24 h P.I (IV), the blood circulation half-life time estimated to be 20.1 h ± 3.4 h	[165]
NIR-I optical imaging	AgInSe ₂ /ZnS	RGD-AP (AP: amphiphilic polymer-octylamine modified poly(acrylic acid))	<20 nm (HD)	775 nm, 20%	IV at 10 mg kg ⁻¹ body weight	Active targeting of RGD-QD to ayb3 integrin receptor overexpressed ayb3-positive MDA-MB-231 breast tumor	[159]
NIR-I optical imaging	InAs/InP/ZnSe	MPA, or MPA+HSA	<10 nm (HD)	800 nm	IV at 200 pmol per animal	Passive targeting of colon tumor, QD-MPA and QD-MPA-HAS both showed high tumor uptake, the former presenting higher RES uptake and lower tumor accumulation than the latter/renal clearance	[166]
NIR-I optical imaging	ZnAgInSe/ZnS	cRGD-Sulfobetaine-PIMA-Histamine	≈55 nm (TEM, QD cluster)	740 nm	IV at 200 μL, ≈10 μg g ⁻¹ of body weight of nude mice	Active targeting to U87MG Glioblastoma and MCF-7 breast cancer tumors through c-RGD conjugation and passive targeting through EPR, high EPR effect and low RES	[167]
NIR-II Optical Imaging	Ag ₂ S	DSPE-PEG, alendronate (Ald), doxorubicin (DOX)	3.8 nm (TEM)	1150 nm	IV at 0.24 mg per animal	Active targeting, chemotherapy of bone Luc-A549 tumor, and inhibition of osteolysis, t _{1/2} = 115 min	[168]
NIR-II Optical Imaging	Ag ₂ S	DHLA-PEG	5.4 nm (TEM), HD (26.8 nm)	1200 nm, 15.5%	IV at 0.268 mg per animal	Passive targeting to 4T1 tumor (>10% ID g ⁻¹) through the EPR effect/biliary clearance	[112]

Table 3. Continued.

Imaging technique	Composition	Surface functionalization	Size	Peak emission and PL QY	Route and dose	Studies, animal model/clearance	References
NIR-II Optical Imaging	Ag ₂ S	Tat-peptide	5.4 nm (TEM)	1200 nm, 15.5%	IV at 1.5 × 10 ⁶ QDs-labeled human mesenchymal stem cells (hMSCs)	In vivo tracking of QDs labeled hMSCs in mice with acute liver failure, in situ translocation and fine distribution of transplanted hMSCs	[113]
NIR-II Optical Imaging	Ag ₂ S	cRGDfk	≈8 nm (HD)	1200 nm	IV	Active targeting to 4T1 luc breast tumor in mice/hepatobiliary and renal clearance	[169]
NIR-II Optical Imaging	Ag ₂ Se	C18-PMH-PEG	2.3 nm (TEM), 21.5 nm (HD)	1300 nm, 29.4%	IV at 6 mg kg ⁻¹ body weight	Deep tissue imaging the liver, spleen, and blood vessels with high spatial resolution of the whole mouse	[161]
VisibleOptical Imaging and MRI	CuInS ₂ /ZnS:Mn	DHLA-PEG2000	3.6 nm (TEM)	610 nm, 27.2%	IV at 0.4 μmol kg ⁻¹ QD	Passive targeting to colon LS180 tumor mice by EPR effect/renal clearance	[68]
PET/CRET	[⁶⁴ Cu]CuInS/ZnS	PEG-GSH	23 nm (HD)	680 nm, 25%	IV (50 μg, 300 μCi)	Active targeting to glioblastoma U87MG tumor mice, highest tumor uptake (10.8% ID g ⁻¹ at 18 h)	[170]

^{a)}Abbreviations: SQ: Subcutaneous; CRET: Cerenkov resonance energy transfer; HD: hydrodynamic diameter; DHLA: dihydroliipoic acid; FA: folic acid; GSH: glutathione.

PEG linker.^[81] Similar to Dubertret's group's work, the addition of the ZnS shell around the core increased the PLQY from just 15% to as high as 60%. The CGKRK peptide binds to p32, which is a mitochondrial protein that is commonly overexpressed by tumor cells. The peptide functionalization increased QD tumor uptake by over two times as compared to QDs functionalized with PEG alone in an MCF10CA1a xenograft of breast cancer mouse model. Similar improvements in tumor uptake were evident in a brain tumor model. QDs were cleared fairly slowly, with a half-life of ≈7 h and remained photostable for the duration of the experiment.

Others have published the synthesis of highly luminescent NIR-I region emitting (≈695 nm) CuInS₂/ZnS core-shell QDs and encapsulated these within folic-acid-functionalized PEGylated phospholipid micelles (QD-FA).^[172] These QD bioconjugates were then used to image pancreatic tumors overexpressing folic acid receptors in mice. The athymic nude mice bearing subcutaneous Pan-1 tumors were intravenously injected with QD-FA. The NIR fluorescent signal can be detected in the tumor region as soon as 15 min post injection and maximum uptake was observed after 30 minutes. Choi et al. synthesized highly photoluminescent NIR (726 nm) Cu_xIn_yS₂/ZnS core-shell QDs with high QY (≈65%) for deep-tissue imaging, which could be useful for assessing cancers below the surface.^[160] Fine tuning of the NIR emission was obtained by adjusting the Cu:In ratio. QDs were encapsulated in poly(methyl methacrylate) (PMMA) using an emulsion/solvent evaporation method and could be visualized through thigh muscle ≈2 mm thick. QDs are also well-suited for use in two-photon imaging applications due to their large absorption cross section.^[22,173] Their advantages have recently been utilized for deep tissue imaging, resulting in high spatial resolution at 300 μm and fast acquisition speeds while allowing for multi-color imaging.^[51] More investigation into the use of QDs in combination with two-photon microscopy is well-warranted for both fundamental and diagnostic purposes.

Even though considerable attention has been paid to the synthesis of CuInS₂ and CuInSe₂ systems, the PLQY of these cores are often fairly low compared to other QD compositions. However, in 2011 Zhang and colleagues synthesized a quaternary QD system ZnAgInSe with PLQY of >70%.^[174] Then, two years later, Deng et al. demonstrated the ability to maintain a PLQY as high as 50% while tuning ZnAgInSe QD emission from 660 to 800 nm in order to reach the NIR-I region that is useful for in vivo imaging by varying the Zn:Ag precursor ratio.^[175] In 2017, Deng et al. then used NIR-I ZnAgInSe/ZnS quaternary core-shell QD nanoparticles with sulfobetaine-poly(isobutylene-*alt*-maleic anhydride)-histimine (SPH) polymer conjugated on the surface for cancer imaging. The histamine coordinates with the metal center, the zwitterionic nature of the exposed sulfobetaine end group provides hydrophilicity, and the PIMA backbone affords improved biocompatibility.^[167] A cyclic RGD peptide was also conjugated to the QD surface in order to target α_vβ₃ integrin cell surface receptors on human malignant glioma cells. These RGD-SPH-QDs self-assemble into clusters and emit at 740 nm after excitation at 450 nm. α_vβ₃⁺ U87MG (glioblastoma) tumor bearing mice or α_vβ₃⁻ MCF-7 (breast cancer) were injected with the RGD-SPH-QDs, and NIR images were taken up to 72 h post-injection (**Figure 3**). The NIR fluorescence intensity reaches an optimum tumor/normal (T/N) enrichment ratio 4–8 h post-injection to the U87MG bearing nude mice and remains high through 60 h. By benefiting from both the active targeting effect of c-RGD and the passive targeting effect of EPR, RGD-SPH QD clusters have demonstrated the ability to quickly and effectively target tumors.

In 2014, Deng et al. published the synthesis of an RGD-modified, octylamine-modified poly(acrylic acid)-wrapped ternary AgInSe₂/ZnS QDs with a composition-tunable PL emission and PLQY of 40%.^[159] They have been used in the in vivo imaging of α_vβ₃⁺ MDA-MB-231 or α_vβ₃⁻ MCF-7 tumor bearing mice. These water-soluble QDs retained their PLQY of 40%.

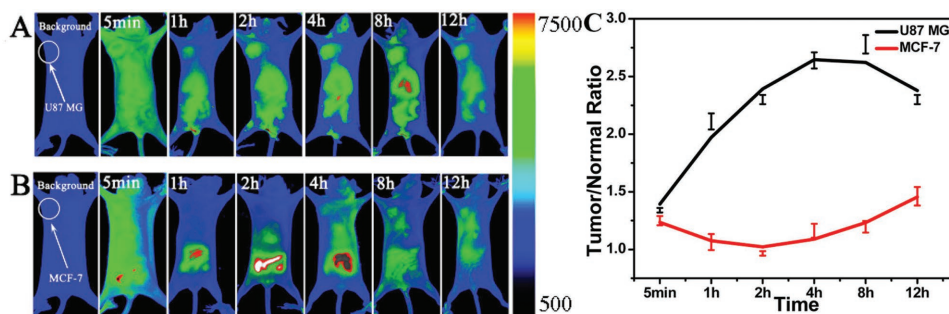


Figure 3. Longitudinal distribution of RGD-SPH ZnAgInSe/ZnS QDs-clusters in nude mice bearing A) $\alpha_v\beta_3^+$ U87MG tumor or B) $\alpha_v\beta_3^-$ MCF-7 tumor (indicated by a white circle), detected using NIR QD imaging ($\lambda_{ex} = 660$ nm, $\lambda_{em} = 740$ nm). C) Corresponding quantification of the ratio between tumor and normal muscle signal. Reproduced with permission.^[167] Copyright 2017, American Chemical Society.

The carboxylic acid groups on the amphiphilic polymer were modified with c-RGD peptide to target $\alpha_v\beta_3$ integrin cell surface receptor on human glioblastoma cells. QDs were injected intravenously at 10 mg kg^{-1} into mice bearing either an $\alpha_v\beta_3^+$ or $\alpha_v\beta_3^-$ tumor. QDs functionalized with $\alpha_v\beta_3$ integrin accumulated in the $\alpha_v\beta_3^+$ tumors while no accumulation was observed in the $\alpha_v\beta_3^-$ tumors.

AgInS₂ ternary QDs with an emission of 800 nm have been synthesized by Liu et al. for tumor imaging at the NIR-I window.^[98] QDs were encapsulated in a poloxamer type polymer pluronic F127. For in vivo tumor imaging studies, radiation induced fibrosarcoma cells were used to develop tumor xenografts subcutaneously on the shoulder of mice. QD encapsulated polymer micelles (3 mg) were administered intravenously and accumulated in tumor 15 min post injection, presumably due to the EPR effect since no active targeting agent was used. After 80 min, QDs started to accumulate in the liver and spleen suggesting the onset of clearance. Similar NIR (817 nm) AgInS₂ ternary QDs were prepared by Tan et al. without any active target design.^[176] The QD surface was modified with capping agent poly(acrylic acid)-graft-mercaptoethylamine (PAA-g-MEA), which has a multidentate molecular structure. For in vivo studies, mice were subcutaneously or intravenously injected with multidentate polymer-capped QDs and excited at 630 nm. For subcutaneously injected QDs, even after 12 h of injection there was little loss in fluorescence intensity while intravenously injected QDs had already been distributed throughout the body within 4 h.

Gao et al. produced mercaptopropionic acid (MPA)-coated InAs/InP/ZnSe QDs that emit in the NIR-I (800 nm) region.^[166] The MPA-capped QDs showed higher tumor uptake as compared to a commercially purchased carboxylic-acid-capped QDs. Differences were attributed to differences in particle diameter, since the smaller MPA-QDs (10 nm) were able to avoid RES uptake and the larger COOH-QDs (25 nm) were not. The differences in surface chemistry were not investigated directly or expected to play a significant role in tumor uptake. The MPA-QDs were then coated with human serum albumin (HSA) with the goal of lowering macrophage uptake. These QDs were intravenously injected into nude mice bearing subcutaneous 22B tumor and LS174T tumors, and demonstrated an increase from 13.5% to 20% of the initial dose per g tissue after coating with HSA.

Yu et al. published one-pot synthesis of CuInS₂/ZnS core-shell QD system at low temperature (160 °C).^[88] These

hydrophobic QDs first underwent ligand exchange with mercaptoundecanoic acid and were subsequently surface conjugated with the single domain antibody EG2 against the epidermal growth factor receptor that is often overexpressed in brain tumor cells. This QD system demonstrated NIR-I region emission of ≈ 790 nm and QY of 8% after bioconjugation. The EG2-conjugated QDs were introduced to nude mice containing an orthotopic brain glioblastoma tumor model, and showed increased fluorescence signal at tumor region compared to nonconjugated QDs.

4.3. Optical Imaging in the NIR-II Region for Primary Tumor Localization

Models of in vivo imaging have shown that utilizing QDs that emit at 1320 nm (NIR-II region) rather than 850 nm (NIR-I region) could improve the overall signal-to-noise ratio by greater than 100-fold, due in part to reduced autofluorescence and superior tissue penetration at those wavelengths.^[28,177,178] Efforts to develop QDs that emit in the NIR-II window have produced an array of heavy element QDs composed of materials such as PbSe, PbS, and CdHgTe.^[179–181] NIR-II QDs have also been synthesized without toxic heavy elements, most commonly with Ag₂S. Wang and co-workers have contributed significantly in the development of various Ag₂S biocompatible QDs. DHLA-PEG modified Ag₂S QDs have an emission ≈ 1200 nm.^[45] The COOH group of the DHLA was modified with an $\alpha_v\beta_3$ integrin targeting peptide (c-RGD peptide) or an epidermal growth factor receptor targeting (EGFR) protein (Erbix). Using in vitro studies, c-RGD modified Ag₂S QDs have been shown to successfully target $\alpha_v\beta_3^+$ EGFR⁻ human glioblastoma (U87 MG) while Erbix-modified Ag₂S QDs target a $\alpha_v\beta_3^-$ EGFR⁺ breast cancer cell line (MDA-MB-468).^[45] Although the DHLA-Ag₂S QDs has a very low QY of 5.8%, it is still considerably higher to the NIR standard dye, IR-26, which has a reference QY of 0.5%. When the DHLA groups on the surface were functionalized further with PEG, the QY further increased up to 15.5%, likely due to the additional protection of the Ag₂S surface by PEG.

Wang and co-workers also synthesized NIR-II emitting Ag₂Se QDs with emission centered around 1300 nm to image microvasculature.^[161] QDs were then conjugated to PEG poly(maleicanhydride-*alt*-1-octadecene) to impart

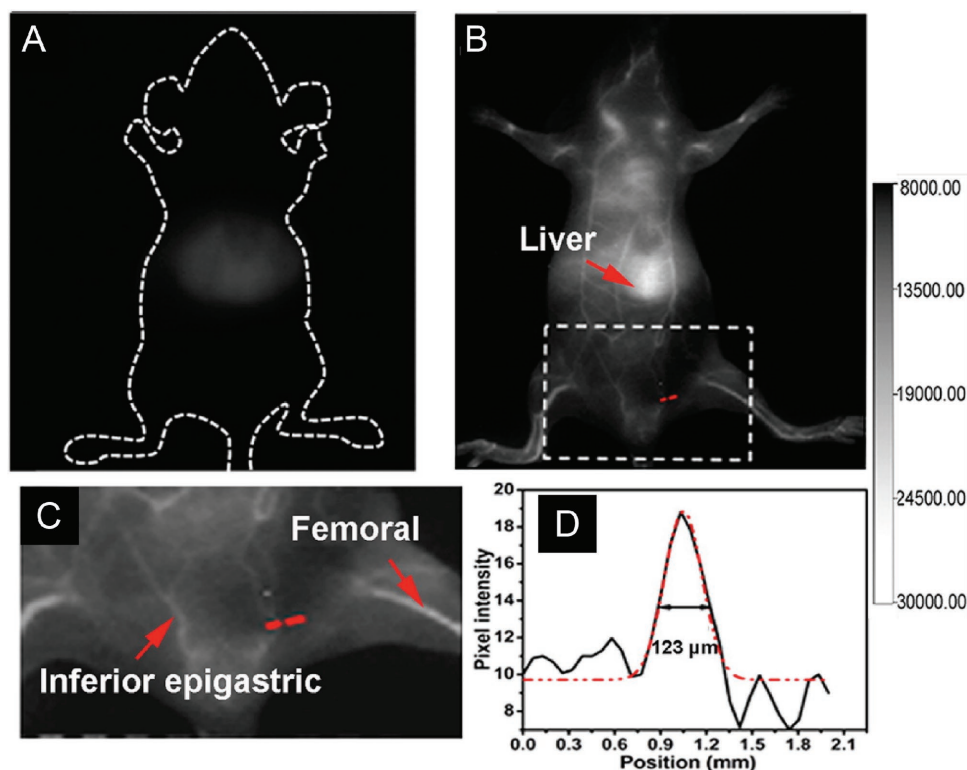


Figure 4. In vivo imaging of live mice in the supine position after 200 μL of A) indocyanine green (3.7 mg mL^{-1}) or B) C18-PMH-PEG- Ag_2Se QDs (0.6 mg mL^{-1}) was injected via the tail vein. C) A magnified image of the selected zone in (B) shows the ability to distinguish fine vasculature on the order of $123 \mu\text{m}$ in diameter. D) A cross-sectional intensity profile measured along the red-dashed line in (C) with its peak fitted to Gaussian functions. The fluorescence signal from the Ag_2Se QDs is easily distinguishable from the endogenous autofluorescence without any image processing. Adapted with permission.^[161] Copyright 2013, American Chemical Society.

biocompatibility and injected intravenously. This strategy enabled the visualization of vasculature and organ structures less than $100 \mu\text{m}$ with high contrast (Figure 4). In comparison, a sixfold higher dose of the indocyanine green resulted in a relatively weak and disperse signal. Achilefu's group synthesized ultrasmall ($<10 \text{ nm}$) Ag_2S QDs and demonstrated the ability to tune emission from $500\text{--}1200 \text{ nm}$.^[169] After functionalizing these QDs with the tumor-targeting peptide cyclic pentapeptide cRGDfK, QDs were injected in 4T1luc tumor-bearing BALB/c mice. These QDs were designed to take advantage of both the EPR effect and an active targeting moiety. They were found to be preferentially distributed in the tumor relative to the kidneys.

4.4. Sentinel Lymph Node Imaging for Diagnosis

In addition to imaging the primary tumor, imaging of SLNs is also extremely important for accurate diagnosis and treatment. Cancer often spreads through the lymphatic system and SLNs are the first to show evidence of metastatic behavior. Current SLN mapping for breast cancer is performed by injecting radiolabeled lymphatic tracers or fluorescent/visible dyes into the tumor which are then cleared via the SLNs. After effectively mapping, a minimally invasive SLN biopsy is performed to determine the stage of the disease, which affects treatment options. Though radiolabeling has the potential to improve

sensitivity, it poses health risks to both the patient and staff and presents logistical disadvantages, such as requiring specialized equipment, access to radioactive material, and a skilled staff. As described in Section 1 above, the three currently approved small molecule fluorescent dyes are rapidly cleared from SLNs and spread quickly throughout the entire lymphatic network before the completion of surgery, making it difficult to identify only the lymph nodes that immediately drain from the tumor.

NIR fluorescence imaging is a potential superior option because it avoids the safety concerns associated with ionizing radiation (CT) or the use of a radioactive tracer (PET) while also enabling real-time visualization of lymph nodes without requiring a greater depth than simple visual inspection. QDs may be able to overcome the issues associated with small molecule dyes as they have demonstrated good localization and retention in the regional lymph system and are resistant to photobleaching. Helle et al. have used NIR fluorescent $\text{CuInSe}_2/\text{ZnS}$ core-shell QDs ($\approx 20 \text{ nm}$), which is in the optimal range for lymphatic drainage^[6] for fluorescence guided SLN mapping in a 4T1 (mammary carcinoma) tumor bearing mice.^[162] QDs (20 pmol) were injected subcutaneously to the right anterior paw, which resulted in a fluorescent signal in the right axillary lymph node that appeared within 5 min of injection and did not begin decreasing in intensity until 8 h later, suggesting the presence of a reasonable imaging time window using this approach. In comparison, technetium-99m, the most

common radioisotope used in medical imaging, has a physical half-life of about 6 h and biological half-life of ≈ 1 d.^[7,182] which combine to reduce the signal by half every 4.8 h. While it is essential for radiation safety reasons that technetium-99m is cleared relatively quickly, biocompatible QDs do not present the same acute safety issue. In addition, QDs remained confined to the regional lymph nodes and did not appear to migrate further into the lymphatic system over the time scale studied (7 d),^[162] thereby identifying only the relevant lymph nodes for biopsy. The larger size of these QDs (20 nm) caused them to be eliminated mainly through hepatobiliary excretion in feces. Indium and its oxide are not expected carcinogens and after SLN removal, the remaining content of indium in the body was ≈ 157 μg (total dose of indium: 900 μg), which is similar to what a typical human ingests over three weeks. Yaghini et al. have used bio-CFQD (InP/ZnS core-shell) QDs to successfully perform ex vivo lymph node mapping.^[158] InP/ZnS QDs were surface functionalized with hexamethoxymethylamine, and further grafted to PEG to prolong blood circulation and reduce RES uptake. Bio-CFQD injected subcutaneously into the paw of Hooded Lister rats concentrated in lymph nodes and remained visible for up to 10 days after administration, which was much longer than the traditional organic dyes that must be administered immediately prior or during the procedure or risk being drained (within hours) from the SLNs before surgery has been completed.

Swihart's group conducted SLN mapping using AuCu_{2-x}Se heterodimer QDs.^[183] Localized surface plasmon resonance (LSPR) has been observed in heavily doped semiconductors including copper chalcogenide QDs which exhibit strong LSPR absorbance in the NIR. These metal-doped copper chalcogenides (Cu_{2-x}Se and Cu_{2-x}S) may be useful for deep tissue

contrast enhancement in photoacoustic imaging due to the ample tissue penetration of NIR light. AuCu_{2-x}Se QDs were made water dispersible by ligand exchange with thiol-PEG. AuCu_{2-x}Se QDs were then used for SLN mapping in a rat using photoacoustic system operating at a wavelength of 1064 nm. SLNs could be visualized up to 70 min after a 400 μg injection of QDs at a depth of up to 1.7 cm, which is of clinical relevance and higher than the 1 cm reported to be the maximum for indocyanine green, the FDA-approved small molecule fluorophore with the most favorable emission wavelength for tissue penetration (Figure 5).^[53]

4.5. Imaging during Surgical Resection

Recent advances in tumor imaging probes and equipment have the potential to revolutionize the field of oncological surgery. The precise and complete removal of the tumor remains challenging due to a myriad of issues including concern over loss-of-function from excessive healthy tissue removal. Highly specific, robust detection of tumors through real-time acquisition of high contrast images has the propensity to reduce or eliminate tumor tissue remaining at the margin after removal and thereby minimize recurrence. Fluorescence imaging presents a unique opportunity for real-time intraoperative imaging because, unlike MRI, CT, and PET, it does not require long collection times and can therefore be used to provide feedback with minimal delay. Fluorescent imaging probes for image-guided surgery require tumor specificity, high PLQY, photostability, and low cytotoxicity. In one clinical study investigating the resection of malignant gliomas, 64% of patients had residual cancer cells at the margin, corresponding to a dramatically

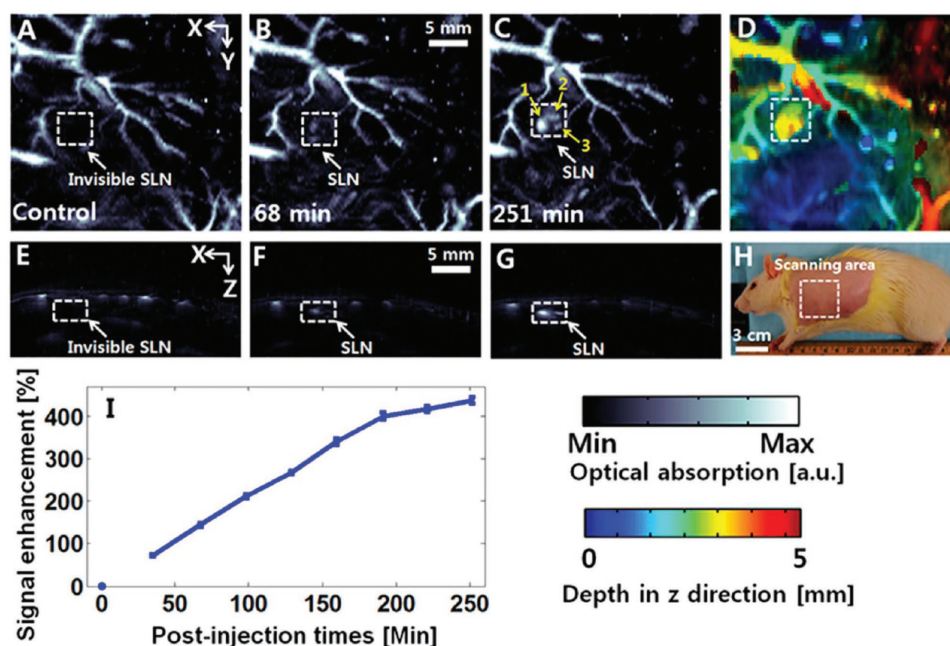


Figure 5. Noninvasive in vivo photoacoustic (PA) time-course coronal maximum amplitude projection (MAP) images. PA images were acquired A) before and B) 68 min and C) 251 min after injection. Three lymph nodes indicated with 1–3 are visible in the axillary region. D) Depth-resolved MAP image of (C). E–G) Cross-sectional PA B-scans of A–C. H) Mouse with hair removed prior to imaging. I) Increase in signal due to accumulation of QDs in SLN over time. Reproduced with permission.^[183] Copyright 2013, American Chemical Society.

increased likelihood of recurrence.^[184] When 5-ALA was used to image the tumor margins during surgery, the proportion of patients with residual tumor cells decreased to 35%, which demonstrates the potential for this approach. However, 5-ALA, methylene blue, and indocyanine green do not inherently demonstrate a high selectivity for cancer tissue over healthy tissue, leading to a lack of contrast at the tumor margin.^[10] Alternatively, QDs modified with tumor targeting motifs have the potential to achieve a strong contrast at the tumor boundary and thereby allow surgeons to monitor and completely excise the tumor. On top of targeting specificity, high PLQY would also be desirable to further improve contrast or reduce the mass of QDs needed per patient. Several recent clinical trials have demonstrated good results using novel non-QD tumor-targeting NIR fluorophores for the improved identification of tumor margins during surgical resection.^[185,186]

4.6. Multimodal Imaging

Multimodal imaging is highly desirable in diagnostics because it can overcome the limitations of single imaging modalities. While this approach often requires two separate contrast agents, some groups have developed QDs that can be imaged using both fluorescence and MRI or PET. Different strategies have been employed to pursue the goal of developing multimodal QD contrast agents by imparting magnetic properties. These strategies can be separated into three categories:^[27] (1) conjugation of magnetic chelates to QDs,^[187] (2) doping with transition metals,^[68] and (3) engineering composite materials by encapsulating magnetic nanoparticles and QDs into inert matrices.^[188] For example, Gao and co-workers reported Mn-doped CuInS₂/ZnS QDs as bimodal imaging probes and showed that the addition of a shell (ZnS) not only enhanced the fluorescence of the core but also protected it from

quenching in the presence of the paramagnetic Mn²⁺ ions.^[68] The 3.6 nm sized QDs were made water-soluble using ligand exchange with DHLA-PEG. These intrinsically magnetic QDs are smaller in size and therefore less prone to accumulation in the reticuloendothelial system compared to nanoparticles >50 nm. For dual imaging, PEGylated CuInS₂/ZnS:Mn was injected intravenously to nude BALB/c mice bearing subcutaneously transplanted with LS180 tumor cells in the flank region of the right hind leg. These multimodal QDs were capable of detecting subcutaneous and intraperitoneal tumors ≈2 mm in diameter through both T₁ weighted MR imaging and fluorescence.

Apart from magnetic/fluorescent bifunctional QD materials, which represent perhaps the most obvious avenue for bimodal imaging, QDs have also been combined with positron emitting material to prepare a unique bifunctional imaging agent. Guo et al. reported the incorporation of a positron-emitting isotope into QDs to generate self-illuminating PET enabled bifunctional nanoprobes.^[170] This novel material requires no external light source due to Cerenkov resonance energy transfer (CRET), which results in luminescence at the point of radionuclide decay. To accomplish this, intrinsically radioactive CuInS₂/ZnS QDs were prepared by incorporating trace amount of ⁶⁴CuCl₂ to the initial reaction mixture. The CuInS₂/ZnS QDs have an excitation spectrum that overlaps well with the Cerenkov luminescence of ⁶⁴Cu, and therefore the QD core can be used as an efficient matrix for CRET. To make the QDs water soluble and biocompatible, the QD surface was functionalized with glutathione (GSH) and methoxy PEG thiol (mPEG). These QDs were intravenously injected to U87MG tumor-bearing mice and imaged with both PET and CRET luminescence (Figure 6). Eighteen hours after injection, the tumor had accumulated over 10% of the injected dose per gram of tissue for the PEGylated QDs, which was over twice that of the GSH functionalized QDs. The obvious drawback of this approach would be the limited

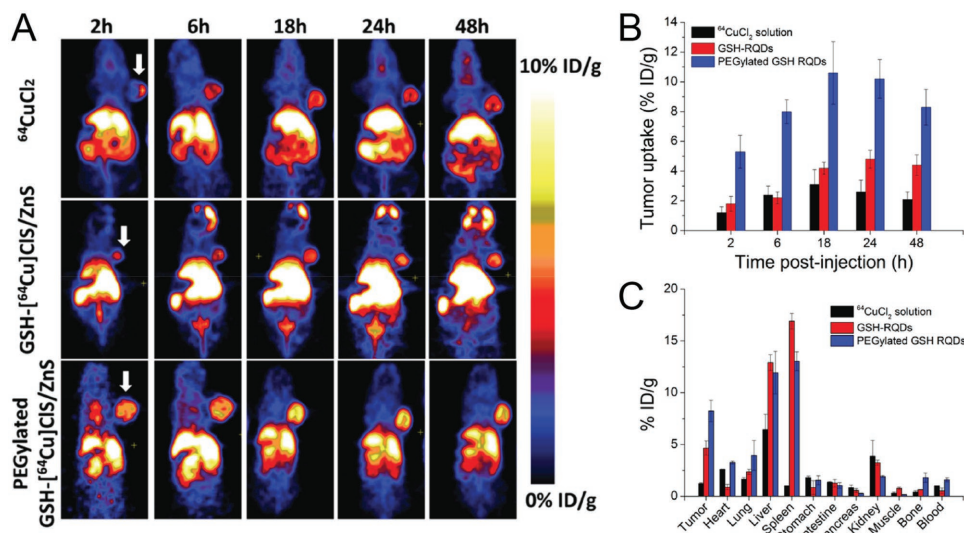


Figure 6. PET imaging of U87MG tumor-bearing mice. A) Representative whole-body coronal PET images at 2, 6, 18, 24, and 48 h after intravenous injection of 100 μ L (50 μ g, 300 μ Ci) of ⁶⁴CuCl₂, GSH-⁶⁴CuInS₂/ZnS and PEGylated GSH-⁶⁴CuInS₂/ZnS QDs. The arrow indicates location of the tumor. B) Graph showing improved tumor uptake by PEGylated QDs and C) distribution of ⁶⁴Cu in organs 48 h after injection, $n = 3$. Reproduced with permission.^[170] Copyright 2014, American Chemical Society.

half-life of PET emitters, such as ^{64}Cu (12.7 h) that would necessitate QD synthesis shortly before use. This represents a major barrier to commercialization on top of the usual radiation exposure concerns and may make the prospect of developing this technology for clinical use untenable. However, using these approaches, it may be possible to use one targeted QD contrast agent for both preoperative and intraoperative tumor characterization.

5. Conclusion

The recent increased interest in optical imaging, particularly for intraoperative imaging, has stimulated the development of preclinical imaging equipment (e.g., PerkinElmer's Solaris).^[12,52,189] QDs in the NIR I biological imaging window have the potential to serve as direct substitutes for current small molecule organic dyes and require only minimal modification to existing imaging fluorescence imaging equipment (e.g., filters) to have an immediate impact on intraoperative imaging during SLN biopsy and tumor resection. In the future, QDs in the NIR II biological imaging window, which have two log-order superior tissue penetration,^[28,177,178] may ultimately offer superior imaging depth that enables noninvasive, high-resolution fluorescence-mediated tomography at clinically relevant depths. However, this will require the development of QDs with high PL QY and upgrading existing imaging equipment with InGaAs detectors that have greater sensitivity for the relevant wavelengths.

5.1. Quantum Dot Biocompatibility

Early preclinical data using conventional (i.e., cadmium-containing) QDs has helped to demonstrate their value as fluorescence imaging probes;^[190] however, as the focus shifts from animal studies to potential clinical use in humans, it has become clear that QDs containing cadmium or other highly toxic elements are extremely unlikely to receive clinical approval.^[191,192] Therefore, future QDs designed for biomedical applications should use materials with superior biocompatibility such as Ag and Cu, which have far lower elemental toxicity while remaining capable of NIR emission. Aside from composition-associated toxicity, size-based toxicity is perhaps an even larger potential concern for clinical translation due to the limited precedence for solid nanoparticle toxicity.^[193] In particular, chronic toxicity due to poor clearance and prolonged residence time (in some cases, two years) will be a key consideration.^[144] As a result, future studies should focus on creating QDs with the appropriate size (<5 nm)^[151] and surface functionalization to promote rapid clearance in urine. Rapid clearance will also have the added benefit of reducing background fluorescence from nontargeted areas of the body during imaging.^[194]

5.2. Standardization of Studies

A major challenge in the use of QDs as imaging probes has been the difficulty comparing these materials produced by

different research groups. Because QDs are synthesized with a wide variety of elements, stoichiometry, synthesis methods, sizes, and surface functionalization strategies, it has been nearly impossible to draw broad conclusions regarding single variable changes on important downstream properties such as fluorescence, biodistribution, biocompatibility, and clearance. In addition, while some studies use adequate controls for *in vivo* studies (e.g., with and without surface modification), others do not, which are missed opportunities to develop fundamental knowledge regarding the benefits of these approaches. Systematic studies controlling for all but one variable would be extremely beneficial for determining their effects on dependent properties. The stepwise nature of QD synthesis should enable systematic control over QD characteristics such as shell thickness and surface modification.

5.3. Molecular Targeting Opportunities

Small QDs with hydrophilic surface modifications appear sufficient for lymph node imaging, but more sophisticated targeting mechanisms are likely required to enhance tumor imaging. The EPR effect alone for tumor targeting is unlikely to provide the contrast required to make QDs useful clinical tools due to its relatively poor selectivity for cancer tissue compared to healthy tissue.^[195] Instead, functionalizing the QD surface with tumor-targeting biomolecules appears to be a more promising strategy. Targeting proteins often upregulated in cancer, or better yet based on patient-specific genetic mutations, would have major implications for imaging in cancer and other diseases. Because current imaging methods are largely confined to assessing tissue morphology, these approaches have limited capacity for detecting early metastases, which may be very small and have similar properties to healthy tissue. However, the potentially high specificity provided by surface-functionalized QDs may enable superior detection of metastases and advanced molecular characterization of tumors to improve cancer diagnosis and selection of therapy.

5.4. Transitioning QDs to the Clinic

Cancer would appear to be a prime application for establishing proof-of-concept QD safety and utility in humans because of its low risk relative to its potential rewards. Since many cancer therapies such as chemotherapy, radiotherapy, and surgical resection are associated with severe side effects, there is likely to be some level of tolerance for QD side effects if they improve tumor characterization and thereby favorably influence treatment selection and prognosis. Nevertheless, early clinical trials are likely to be limited to patients with extremely poor prognosis to minimize the magnitude of adverse outcomes. This strategy has been used previously for first-in-human cancer therapies with good success and may represent the safest path towards QD commercialization for cancer and other potential biomedical imaging and therapeutic applications.

Once safety has been established, the first application of QDs for cancer imaging is likely to be Ag- or Cu-based QDs in

the NIR I biological imaging window for intraoperative lymph node mapping or shallow (<2 cm) imaging of the most easily accessible external and internal surfaces (e.g., skin, gastrointestinal tract) where resolution remains high due to limited scattering.^[28,196] The parallel development of improved detectors, 3D deconvolution, spectral unmixing, and reconstruction algorithms will also aid in the adoption of QDs for deeper tissue imaging using fluorescence-mediated tomography. Long-term, QD may also serve additional roles such as probes for multiplexed characterization of the tumor microenvironment,^[197] targeted drug delivery,^[198] photodynamic therapy,^[199] or photothermal therapy.^[140] Ultimately, the goals of QD design should be to avoid adverse reactions, demonstrate a high preference for tumors or lymph nodes compared to healthy tissue, exhibit strong and stable fluorescence within the near-infrared biological imaging windows, and be cleared by the body over a duration that is sufficiently long to retain optimal contrast during surgery, but then be completely cleared soon after.

Conflict of Interest

The authors declare no conflict of interest.

Keywords

cancer imaging, fluorescence, near-infrared, optical imaging, quantum dots

Received: November 2, 2017

Revised: November 26, 2017

Published online: February 22, 2018

- [1] S. Tang, Q. S. Cai, H. Chibli, V. Allagadda, J. L. Nadeau, G. D. Mayer, *Toxicol. Appl. Pharmacol.* **2013**, 272, 443.
- [2] R. L. Siegel, K. D. Miller, A. Jemal, *Ca Cancer J. Clin.* **2017**, 67, 7.
- [3] R. A. Smith, K. S. Andrews, D. Brooks, S. A. Fedewa, D. Manassaram-Baptiste, D. Saslow, O. W. Brawley, R. C. Wender, *Ca Cancer J. Clin.* **2017**, 67, 100.
- [4] S. I. Kubota, K. Takahashi, J. Nishida, Y. Morishita, S. Ehata, K. Tainaka, K. Miyazono, H. R. Ueda, *Cell Rep.* **2017**, 20, 236.
- [5] M. L. James, S. S. Gambhir, *Physiol. Rev.* **2012**, 92, 897.
- [6] L. Fass, *Mol. Oncol.* **2008**, 2, 115.
- [7] K. Schwachau, in *Technetium: Chemistry and Radiopharmaceutical Applications*, Wiley-VCH, New York **2007**, p. 371.
- [8] A. L. Vahrmeijer, M. Hutteman, J. R. van der Vorst, C. J. H. van de Velde, J. V. Frangioni, *Nat. Rev. Clin. Oncol.* **2013**, 10, 507.
- [9] R. Weissleder, M. J. Pittet, *Nature* **2008**, 452, 580.
- [10] R. R. Zhang, A. B. Schroeder, J. J. Grudzinski, E. L. Rosenthal, J. M. Warram, A. N. Pinchuk, K. W. Eliceiri, J. S. Kuo, J. P. Weichert, *Nat. Rev. Clin. Oncol.* **2017**, 14, 347.
- [11] S. S. Kartha, C. E. Chacko, J. M. Bumpous, M. Fleming, E. J. Lentsch, M. B. Flynn, *Otolaryngol. Head Neck Surg.* **2006**, 135, 765.
- [12] S. B. Mondal, S. Gao, N. Zhu, R. Liang, V. Gruev, S. Achilefu, *Adv. Cancer Res.* **2014**, 124, 171.
- [13] U. Resch-Genger, M. Grabolle, S. Cavaliere-Jaricot, R. Nitschke, T. Nann, *Nat. Methods* **2008**, 5, 763.
- [14] S. Q. Feng, J. Chen, Y. Wo, Y. X. Li, S. Y. Chen, Y. X. Zhang, W. J. Zhang, *Biomaterials* **2016**, 103, 256.
- [15] V. Ntziachristos, *Nat. Methods* **2010**, 7, 603.
- [16] F. Helmchen, W. Denk, *Nat. Methods* **2005**, 2, 932.
- [17] L. V. Wang, *Nat. Photonics* **2009**, 3, 503.
- [18] Q. T. Nguyen, R. Y. Tsien, *Nat. Rev. Cancer* **2013**, 13, 653.
- [19] Y. Park, S. Jeong, S. Kim, *J. Photochem. Photobiol., C* **2017**, 30, 51.
- [20] F. Leblond, S. C. Davis, P. A. Valdes, B. W. Pogue, *J. Photochem. Photobiol., B* **2010**, 98, 77.
- [21] I. L. Medintz, H. T. Uyeda, E. R. Goldman, H. Mattoussi, *Nat. Mater.* **2005**, 4, 435.
- [22] X. Michalet, F. F. Pinaud, L. A. Bentolila, J. M. Tsay, S. Doose, J. J. Li, G. Sundaresan, A. M. Wu, S. S. Gambhir, S. Weiss, *Science* **2005**, 307, 538.
- [23] C. E. Probst, P. Zrazhevskiy, V. Bagalkot, X. H. Gao, *Adv. Drug Delivery Rev.* **2013**, 65, 703.
- [24] N. Hildebrandt, C. M. Spillmann, W. R. Algar, T. Pons, M. H. Stewart, E. Oh, K. Susumu, S. A. Diaz, J. B. Delehanty, I. L. Medintz, *Chem. Rev.* **2017**, 117, 536.
- [25] J. Zhou, Y. Yang, C. Zhang, *Chem. Rev.* **2015**, 115, 11669.
- [26] K. D. Wegner, N. Hildebrandt, *Chem. Soc. Rev.* **2015**, 44, 4792.
- [27] L. H. Jing, K. Ding, S. V. Kershaw, I. M. Kempson, A. L. Rogach, M. Y. Gao, *Adv. Mater.* **2014**, 26, 6367.
- [28] A. M. Smith, M. C. Mancini, S. Nie, *Nat. Nano* **2009**, 4, 710.
- [29] H. Z. Zhong, Z. L. Bai, B. S. Zou, *J. Phys. Chem. Lett.* **2012**, 3, 3167.
- [30] E. Cassette, M. Helle, L. Bezdetsnaya, F. Marchal, B. Dubertret, T. Pons, *Adv. Drug Delivery Rev.* **2013**, 65, 719.
- [31] J. Kolny-Olesiak, H. Weller, *ACS Appl. Mater. Interfaces* **2013**, 5, 12221.
- [32] L. H. Jing, S. V. Kershaw, Y. L. Li, X. Huang, Y. Y. Li, A. L. Rogach, M. Y. Gao, *Chem. Rev.* **2016**, 116, 10623.
- [33] D. Aldakov, A. Lefrancois, P. Reiss, *J. Mater. Chem. C* **2013**, 1, 3756.
- [34] P. Reiss, M. Carriere, C. Lincheneau, L. Vaure, S. Tamang, *Chem. Rev.* **2016**, 116, 10731.
- [35] M. Sandroni, K. D. Wegner, D. Aldakov, P. Reiss, *ACS Energy Lett.* **2017**, 2, 1076.
- [36] K. E. Knowles, K. H. Hartstein, T. B. Kilburn, A. Marchioro, H. D. Nelson, P. J. Whitham, D. R. Gamelin, *Chem. Rev.* **2016**, 116, 10820.
- [37] G. X. Xu, S. W. Zeng, B. T. Zhang, M. T. Swihart, K. T. Yong, P. N. Prasad, *Chem. Rev.* **2016**, 116, 12234.
- [38] C. Coughlan, M. Ibanez, O. Dobrozhan, A. Singh, A. Cabot, K. M. Ryan, *Chem. Rev.* **2017**, 117, 5865.
- [39] P. M. Allen, M. G. Bawendi, *J. Am. Chem. Soc.* **2008**, 130, 9240.
- [40] R. G. Xie, M. Rutherford, X. G. Peng, *J. Am. Chem. Soc.* **2009**, 131, 5691.
- [41] M. A. Langevin, A. M. Ritcey, C. Ni Allen, *ACS Nano* **2014**, 8, 3476.
- [42] B. K. Chen, H. Z. Zhong, W. Q. Zhang, Z. A. Tan, Y. F. Li, C. R. Yu, T. Y. Zhai, Y. S. Bando, S. Y. Yang, B. S. Zou, *Adv. Funct. Mater.* **2012**, 22, 2081.
- [43] L. Li, A. Pandey, D. J. Werder, B. P. Khanal, J. M. Pietryga, V. I. Klimov, *J. Am. Chem. Soc.* **2011**, 133, 1176.
- [44] Y. Liu, D. Yao, L. Shen, H. Zhang, X. D. Zhang, B. Yang, *J. Am. Chem. Soc.* **2012**, 134, 7207.
- [45] Y. Zhang, G. Hong, Y. Zhang, G. Chen, F. Li, H. Dai, Q. Wang, *ACS Nano* **2012**, 6, 3695.
- [46] H. D. Zang, H. B. Li, N. S. Makarov, K. A. Velizhanin, K. F. Wu, Y. S. Park, V. I. Klimov, *Nano Lett.* **2017**, 17, 1787.
- [47] Y. P. Gu, R. Cui, Z. L. Zhang, Z. X. Xie, D. W. Pang, *J. Am. Chem. Soc.* **2012**, 134, 79.
- [48] R. Weissleder, *Nat. Biotechnol.* **2001**, 19, 316.
- [49] J. Y. Zhao, G. Chen, Y. P. Gu, R. Cui, Z. L. Zhang, Z. L. Yu, B. Tang, Y. F. Zhao, D. W. Pang, *J. Am. Chem. Soc.* **2016**, 138, 1893.
- [50] S. H. Yun, S. J. J. Kwok, *Nat. Biomed. Eng.* **2017**, 1, 0008.

- [51] O. T. Bruns, T. S. Bischof, D. K. Harris, D. Franke, Y. Shi, L. Riedemann, A. Bartelt, F. B. Jaworski, J. A. Carr, C. J. Rowlands, M. W. B. Wilson, O. Chen, H. Wei, G. W. Hwang, D. M. Montana, I. Coropceanu, O. B. Achorn, J. Kloepper, J. Heeren, P. T. C. So, D. Fukumura, K. F. Jensen, R. K. Jain, M. G. Bawendi, *Nat. Biomed. Eng.* **2017**, *1*, 0056.
- [52] V. Ntziachristos, C. Bremer, R. Weissleder, *Eur. Radiol.* **2003**, *13*, 195.
- [53] T. Kitai, in *ICG Fluorescence Imaging and Navigation Surgery* (Ed: M. Kusano), Springer, New York **2016**, 101.
- [54] E. Hemmer, A. Benayas, F. Legare, F. Vetrone, *Nanoscale Horiz.* **2016**, *1*, 168.
- [55] A. L. Antaris, H. Chen, S. Diao, Z. R. Ma, Z. Zhang, S. J. Zhu, J. Wang, A. X. Lozano, Q. L. Fan, L. L. Chew, M. Zhu, K. Cheng, X. C. Hong, H. J. Dai, Z. Cheng, *Nat. Commun.* **2017**, *8*, 15269.
- [56] J. Qi, Y. Fang, R. T. K. Kwok, X. Y. Zhang, X. L. Hu, J. W. Y. Lam, D. Ding, B. Z. Tang, *ACS Nano* **2017**, *11*, 7177.
- [57] Y. Jung, S. Jeong, W. Nayoun, B. Ahn, J. Kwag, S. G. Kim, S. Kim, *J. Biomed. Opt.* **2015**, *20*, 46012.
- [58] A. J. Shuhendler, P. Prasad, H. K. C. Chan, C. R. Gordijo, B. Soroushian, M. Kolios, K. Yu, P. J. O'Brien, A. M. Rauth, X. Y. Wu, *ACS Nano* **2011**, *5*, 1958.
- [59] X. Dang, L. Gu, J. Qi, S. Correa, G. Zhang, A. M. Belcher, P. T. Hammond, *Proc Natl Acad Sci USA* **2016**, *113*, 5179.
- [60] D. Kim, N. Lee, Y. I. Park, T. Hyeon, *Bioconjugate Chem.* **2017**, *28*, 115.
- [61] X. G. Peng, M. C. Schlamp, A. V. Kadavanich, A. P. Alivisatos, *J. Am. Chem. Soc.* **1997**, *119*, 7019.
- [62] B. O. Dabbousi, V. Rodriguez, J. R. Heine, H. Mattoussi, R. Ober, K. F. Jensen, M. G. Bawendi, *J. Phys. Chem. B* **1997**, *101*, 9463.
- [63] M. Bruchez, M. Moronne, P. Gin, S. Weiss, A. P. Alivisatos, *Science* **1998**, *281*, 2013.
- [64] W. C. W. Chan, S. M. Nie, *Science* **1998**, *281*, 2016.
- [65] P. Reiss, M. Protière, L. Li, *Small* **2009**, *5*, 154.
- [66] L. H. Jing, K. Ding, S. Kalytchuk, Y. Wang, R. R. Qiao, S. V. Kershaw, A. L. Rogach, M. Y. Gao, *J. Phys. Chem. C* **2013**, *117*, 18752.
- [67] L. H. Jing, S. V. Kershaw, T. Kipp, S. Kalytchuk, K. Ding, J. F. Zeng, M. X. Jiao, X. Y. Sun, A. Mews, A. L. Rogach, M. Y. Gao, *J. Am. Chem. Soc.* **2015**, *137*, 2073.
- [68] K. Ding, L. H. Jing, C. Y. Liu, Y. Hou, M. Y. Gao, *Biomaterials* **2014**, *35*, 1608.
- [69] L. Li, T. J. Daou, I. Texier, T. T. Kim Chi, N. Q. Liem, P. Reiss, *Chem. Mater.* **2009**, *21*, 2422.
- [70] H. B. Bao, Y. J. Gong, Z. Li, M. Y. Gao, *Chem. Mater.* **2004**, *16*, 3853.
- [71] A. Gerega, N. Zolek, T. Soltysinski, D. Milej, P. Sawosz, B. Toczyłowska, A. Liebert, *J. Biomed. Opt.* **2011**, *16*, 067010.
- [72] T. Pons, E. Pic, N. Lequeux, E. Cassette, L. Bezdetsnaya, F. Guillemin, F. Marchal, B. Dubertret, *ACS Nano* **2010**, *4*, 2531.
- [73] L. De Trizio, L. Manna, *Chem. Rev.* **2016**, *116*, 10852.
- [74] J. Du, Z. L. Du, J. S. Hu, Z. X. Pan, Q. Shen, J. K. Sung, D. H. Long, H. Dong, L. T. Sun, X. H. Zhong, L. J. Wan, *J. Am. Chem. Soc.* **2016**, *138*, 4201.
- [75] X. Gao, Y. Cui, R. M. Levenson, L. W. K. Chung, S. Nie, *Nat. Biotechnol.* **2004**, *22*, 969.
- [76] P. Zrazhevskiy, X. H. Gao, *Nat. Commun.* **2013**, *4*, 1619.
- [77] M. Howarth, K. Takao, Y. Hayashi, A. Y. Ting, *Proc. Natl. Acad. Sci. USA* **2005**, *102*, 7583.
- [78] B. R. Knudsen, M. L. Jepsen, Y. P. Ho, *Expert Rev. Mol. Diagn.* **2013**, *13*, 367.
- [79] A. Orte, J. M. Alvarez-Pez, M. J. Ruedas-Rama, *ACS Nano* **2013**, *7*, 6387.
- [80] J. Aldana, N. Lavelle, Y. J. Wang, X. G. Peng, *J. Am. Chem. Soc.* **2005**, *127*, 2496.
- [81] X. Y. Liu, G. B. Braun, H. Z. Zhong, D. J. Hall, W. L. Han, M. D. Qin, C. Z. Zhao, M. N. Wang, Z. G. She, C. B. Cao, M. J. Sailor, W. B. Stallcup, E. Ruoslahti, K. N. Sugahara, *Adv. Funct. Mater.* **2016**, *26*, 267.
- [82] V. Lesnyak, N. Gaponik, A. Eychmuller, *Chem. Soc. Rev.* **2013**, *42*, 2905.
- [83] A. S. Karakoti, R. Shukla, R. Shanker, S. Singh, *Adv. Colloid Interface Sci.* **2015**, *215*, 28.
- [84] R. Bilan, F. Fleury, I. Nabiey, A. Sukhanova, *Bioconjugate Chem.* **2015**, *26*, 609.
- [85] E. Blanco, H. Shen, M. Ferrari, *Nat. Biotechnol.* **2015**, *33*, 941.
- [86] C. Y. Liu, Y. F. Qi, R. R. Qiao, Y. Hou, K. Y. Chan, Z. Q. Li, J. Y. Huang, L. H. Jing, J. Du, M. Y. Gao, *Nanoscale* **2016**, *8*, 12579.
- [87] K. T. Yong, Y. C. Wang, I. Roy, H. Rui, M. T. Swihart, W. C. Law, S. K. Kwak, L. Ye, J. W. Liu, S. D. Mahajan, J. L. Reynolds, *Theranostics* **2012**, *2*, 681.
- [88] W. Liu, S. P. Zhang, L. X. Wang, C. Qu, C. W. Zhang, L. Hong, L. Yuan, Z. H. Huang, Z. Wang, S. J. Liu, G. B. Jiang, *Plos One* **2011**, *6*, 7.
- [89] I. Corazzari, A. Gilardino, S. Dalmazzo, B. Fubini, D. Lovisolo, *Toxicol. In Vitro* **2013**, *27*, 752.
- [90] K. G. Li, J. T. Chen, S. S. Bai, X. Wen, S. Y. Song, Q. Yu, J. Li, Y. Q. Wang, *Toxicol. In Vitro* **2009**, *23*, 1007.
- [91] F. M. Winnik, D. Maysinger, *Acc. Chem. Res.* **2013**, *46*, 672.
- [92] B. A. Rzigalinski, J. S. Strobl, *Toxicol. Appl. Pharmacol.* **2009**, *238*, 280.
- [93] D. Mo, L. Hu, G. M. Zeng, G. Q. Chen, J. Wan, Z. G. Yu, Z. Z. Huang, K. He, C. Zhang, M. Cheng, *Appl. Microbiol. Biotechnol.* **2017**, *101*, 2713.
- [94] A. Navas-Acien, E. Selvin, A. R. Sharrett, E. Calderon-Aranda, E. Silbergeld, E. Guallar, *Circulation* **2004**, *109*, 3196.
- [95] D. Painuly, A. Bhatt, V. K. Krishnan, *J. Biomed. Nanotechnol.* **2013**, *9*, 257.
- [96] V. Karabanovas, E. Zakarevicius, A. Sukackaite, G. Streckyte, R. Rotomskis, *Photochem. Photobiol. Sci.* **2008**, *7*, 725.
- [97] E. Oh, R. Liu, A. Nel, K. B. Gemill, M. Bilal, Y. Cohen, I. L. Medintz, *Nat. Nanotechnol.* **2016**, *11*, 479.
- [98] L. W. Liu, R. Hu, I. Roy, G. M. Lin, L. Ye, J. L. Reynolds, J. W. Liu, J. Liu, S. A. Schwartz, X. H. Zhang, K. T. Yong, *Theranostics* **2013**, *3*, 109.
- [99] Y. Zhang, Y. J. Zhang, G. S. Hong, W. He, K. Zhou, K. Yang, F. Li, G. C. Chen, Z. Liu, H. J. Dai, Q. B. Wang, *Biomaterials* **2013**, *34*, 3639.
- [100] L. W. Liu, R. Hu, W. C. Law, I. Roy, J. Zhu, L. Ye, S. Y. Hu, X. H. Zhang, K. T. Yong, *Analyst* **2013**, *138*, 6144.
- [101] B. R. Smith, S. S. Gambhir, *Chem. Rev.* **2017**, *117*, 901.
- [102] Y. P. Du, B. Xu, T. Fu, M. Cai, F. Li, Y. Zhang, Q. B. Wang, *J. Am. Chem. Soc.* **2010**, *132*, 1470.
- [103] Y. J. Zhang, Y. S. Liu, C. Y. Li, X. Y. Chen, Q. B. Wang, *J. Phys. Chem. C* **2014**, *118*, 4918.
- [104] R. J. Gui, A. J. Wan, X. F. Liu, W. Yuan, H. Jin, *Nanoscale* **2014**, *6*, 5467.
- [105] P. Jiang, Z. Q. Tian, C. N. Zhu, Z. L. Zhang, D. W. Pang, *Chem. Mater.* **2012**, *24*, 3.
- [106] P. Jiang, C. N. Zhu, Z. L. Zhang, Z. Q. Tian, D. W. Pang, *Biomaterials* **2012**, *33*, 5130.
- [107] H.-Y. Yang, Y.-W. Zhao, Z.-Y. Zhang, H.-M. Xiong, S.-N. Yu, *Nanotechnology* **2013**, *24*, 055706.
- [108] H. Doh, S. Hwang, S. Kim, *Chem. Mater.* **2016**, *28*, 8123.
- [109] I. Hocaoglu, M. N. Cizmeciyan, R. Erdem, C. Ozen, A. Kurt, A. Sennaroglu, H. Y. Acar, *J. Mater. Chem.* **2012**, *22*, 14674.
- [110] C. X. Wang, Y. Wang, L. Xu, D. Zhang, M. X. Li, X. W. Li, H. C. Sun, Q. Lin, B. Yang, *Small* **2012**, *8*, 3137.
- [111] C. Y. Li, L. M. Cao, Y. J. Zhang, P. W. Yi, M. Wang, B. Tan, Z. W. Deng, D. M. Wu, Q. B. Wang, *Small* **2015**, *11*, 4517.

- [112] G. Hong, J. T. Robinson, Y. Zhang, S. Diao, A. L. Antaris, Q. Wang, H. Dai, *Angew. Chem., Int. Ed. Engl.* **2012**, *51*, 9818.
- [113] G. C. Chen, F. Tian, Y. Zhang, Y. J. Zhang, C. Y. Li, Q. B. Wang, *Adv. Funct. Mater.* **2014**, *24*, 2481.
- [114] A. Sahu, A. Khare, D. D. Deng, D. J. Norris, *Chem. Commun.* **2012**, *48*, 5458.
- [115] M. Yarema, S. Pichler, M. Sytnyk, R. Seyrkammer, R. T. Lechner, G. Fritz-Popovski, D. Jarzab, K. Szendrei, R. Resel, O. Korovyanko, M. A. Loi, O. Paris, G. Hesser, W. Heiss, *ACS Nano* **2011**, *5*, 3758.
- [116] L. J. Tan, A. J. Wan, T. T. Zhao, R. Huang, H. L. Li, *ACS Appl. Mater. Interfaces* **2014**, *6*, 6217.
- [117] C. N. Zhu, P. Jiang, Z. L. Zhang, D. L. Zhu, Z. Q. Tian, D. W. Pang, *ACS Appl. Mater. Interfaces* **2013**, *5*, 1186.
- [118] C. Y. Ji, Y. Zhang, T. Q. Zhang, W. Y. Liu, X. Y. Zhang, H. Z. Shen, Y. Wang, W. Z. Gao, Y. D. Wang, J. Zhao, W. W. Yu, *J. Phys. Chem. C* **2015**, *119*, 13841.
- [119] B. H. Dong, C. Y. Li, G. C. Chen, Y. J. Zhang, Y. Zhang, M. J. Deng, Q. B. Wang, *Chem. Mater.* **2013**, *25*, 2503.
- [120] C. Chen, X. W. He, L. Gao, N. Ma, *ACS Appl. Mater. Interfaces* **2013**, *5*, 1149.
- [121] H. Jin, R. J. Gui, J. Sun, Y. F. Wang, *Colloids Surf. B* **2016**, *143*, 118.
- [122] H. Z. Zhong, Y. Zhou, M. F. Ye, Y. J. He, J. P. Ye, C. He, C. H. Yang, Y. F. Li, *Chem. Mater.* **2008**, *20*, 6434.
- [123] E. Cassette, T. Pons, C. Bouet, M. Helle, L. Bezdetsnaya, F. Marchal, B. Dubertret, *Chem. Mater.* **2010**, *22*, 6117.
- [124] H. Z. Zhong, Z. B. Wang, E. Bovero, Z. H. Lu, F. C. J. M. van Veggel, G. D. Scholes, *J. Phys. Chem. C* **2011**, *115*, 12396.
- [125] O. Yarema, D. Bozyigit, I. Rousseau, L. Nowack, M. Yarema, W. Heiss, V. Wood, *Chem. Mater.* **2013**, *25*, 3753.
- [126] X. J. Kang, Y. C. Yang, L. J. Huang, Y. Tao, L. Wang, D. C. Pan, *Green Chem.* **2015**, *17*, 4482.
- [127] Y. Hamanaka, T. Ogawa, M. Tsuzuki, T. Kuzuya, *J. Phys. Chem. C* **2011**, *115*, 1786.
- [128] T. Torimoto, T. Adachi, K.-i. Okazaki, M. Sakuraoka, T. Shibayama, B. Ohtani, A. Kudo, S. Kuwabata, *J. Am. Chem. Soc.* **2007**, *129*, 12388.
- [129] M. L. Dai, S. Ogawa, T. Kameyama, K. Okazaki, A. Kudo, S. Kuwabata, Y. Tsuboi, T. Torimoto, *J. Mater. Chem.* **2012**, *22*, 12851.
- [130] X. J. Kang, L. J. Huang, Y. C. Yang, D. C. Pan, *J. Phys. Chem. C* **2015**, *119*, 7933.
- [131] B. D. Mao, C. H. Chuang, C. McCleese, J. J. Zhu, C. Burda, *J. Phys. Chem. C* **2014**, *118*, 13883.
- [132] D. W. Deng, L. Z. Qu, Y. Q. Gu, *J. Mater. Chem. C* **2014**, *2*, 7077.
- [133] Y. Hamanaka, K. Ozawa, T. Kuzuya, *J. Phys. Chem. C* **2014**, *118*, 14562.
- [134] D. Yao, H. W. Liu, Y. Liu, C. W. Dong, K. Zhang, Y. Sheng, J. L. Cui, H. Zhang, B. Yang, *Nanoscale* **2015**, *7*, 18570.
- [135] O. Yarema, M. Yarema, D. Bozyigit, W. M. M. Lin, V. Wood, *ACS Nano* **2015**, *9*, 11134.
- [136] K. T. Yong, W. C. Law, R. Hu, L. Ye, L. W. Liu, M. T. Swihart, P. N. Prasad, *Chem. Soc. Rev.* **2013**, *42*, 1236.
- [137] S. J. Cho, D. Maysinger, M. Jain, B. Roder, S. Hackbarth, F. M. Winnik, *Langmuir* **2007**, *23*, 1974.
- [138] N. Chen, Y. He, Y. Su, X. Li, Q. Huang, H. Wang, X. Zhang, R. Tai, C. Fan, *Biomaterials* **2012**, *33*, 1238.
- [139] L. Liu, Y.-Y. Xiao, Y.-H. Ji, M.-Z. Liu, Y. Chen, Y.-L. Zeng, Y.-G. Zhang, L. Jin, *Comp. Biochem. Physiol., Part C: Toxicol. Pharmacol.* **2017**, *198*, 19.
- [140] J. H. Li, Y. Zhang, Q. Xiao, F. F. Tian, X. R. Liu, R. Li, G. Y. Zhao, F. L. Jiang, Y. Liu, *J. Hazard. Mater.* **2011**, *194*, 440.
- [141] L. Lai, Y. P. Li, P. Mei, W. Chen, F. L. Jiang, Y. Liu, *J. Membr. Biol.* **2016**, *249*, 757.
- [142] C. Zhou, M. Long, Y. P. Qin, X. K. Sun, J. Zheng, *Angew. Chem., Int. Ed.* **2011**, *50*, 3168.
- [143] L. Vroman, A. L. Adams, *J. Biomed. Mater. Res.* **1969**, *3*, 43.
- [144] B. Ballou, L. A. Ernst, S. Andreko, T. Harper, J. A. J. Fitzpatrick, A. S. Waggoner, M. P. Bruchez, *Bioconjugate Chem.* **2007**, *18*, 389.
- [145] Y. H. Lu, S. C. Xu, H. Y. Chen, M. D. He, Y. C. Deng, Z. W. Cao, H. F. Pi, C. H. Chen, M. Li, Q. L. Ma, P. Gao, Y. Ji, L. Zhang, Z. P. Yu, Z. Zhou, *Biomaterials* **2016**, *90*, 27.
- [146] T. Zhang, Y. Y. Hu, M. Tang, L. Kong, J. L. Ying, T. S. Wu, Y. Y. Xue, Y. P. Pu, *Int. J. Mol. Sci.* **2015**, *16*, 23279.
- [147] Y. N. Zhang, W. Poon, A. J. Tavares, I. D. McGilvray, W. C. W. Chan, *J. Controlled Release* **2016**, *240*, 332.
- [148] C. D. Walkey, J. B. Olsen, H. Guo, A. Emili, W. C. W. Chan, *J. Am. Chem. Soc.* **2012**, *134*, 2139.
- [149] O. Lunov, V. Zablotskii, T. Syrovets, C. Röcker, K. Tron, G. U. Nienhaus, T. Simmet, *Biomaterials* **2011**, *32*, 547.
- [150] C. Liu, Z. Gao, J. Zeng, Y. Hou, F. Fang, Y. Li, R. Qiao, L. Shen, H. Lei, W. Yang, M. Gao, *ACS Nano* **2013**, *7*, 7227.
- [151] H. S. Choi, W. Liu, P. Misra, E. Tanaka, J. P. Zimmer, B. I. Ipe, M. G. Bawendi, J. V. Frangioni, *Nat. Biotechnol.* **2007**, *25*, 1165.
- [152] S. Y. Yang, S. S. Sun, C. Zhou, G. Y. Hao, J. B. Liu, S. Ramezani, M. X. Yu, X. K. Sun, J. Zheng, *Bioconjugate Chem.* **2015**, *26*, 511.
- [153] C. Alric, I. Miladi, D. Kryza, J. Taleb, F. Lux, R. Bazzi, C. Billotey, M. Janier, P. Perriat, S. Roux, O. Tillement, *Nanoscale* **2013**, *5*, 5930.
- [154] Z. J. Zhou, L. R. Wang, X. Q. Chi, J. F. Bao, L. J. Yang, W. X. Zhao, Z. Chen, X. M. Wang, X. Y. Chen, J. H. Gao, *ACS Nano* **2013**, *7*, 3287.
- [155] S.-H. Cheng, F.-C. Li, J. S. Souris, C.-S. Yang, F.-G. Tseng, H.-S. Lee, C.-T. Chen, C.-Y. Dong, L.-W. Lo, *ACS Nano* **2012**, *6*, 4122.
- [156] H. Tang, S. T. Yang, Y. F. Yang, D. M. Ke, J. H. Liu, X. Chen, H. F. Wang, Y. F. Liu, *ACS Appl. Mater. Interfaces* **2016**, *8*, 17859.
- [157] J. B. Liu, M. X. Yu, X. H. Ning, C. Zhou, S. Y. Yang, J. Zheng, *Angew. Chem., Int. Ed.* **2013**, *52*, 12572.
- [158] E. Yaghini, H. D. Turner, A. M. Le Marois, K. Suhling, I. Naasani, A. J. MacRobert, *Biomaterials* **2016**, *104*, 182.
- [159] D. Deng, L. Qu, Y. Gu, *J. Mater. Chem. C* **2014**, *2*, 7077.
- [160] H. S. Choi, Y. Kim, J. C. Park, M. H. Oh, D. Y. Jeon, Y. S. Nam, *RSC Adv.* **2015**, *5*, 43449.
- [161] B. Dong, C. Li, G. Chen, Y. Zhang, Y. Zhang, M. Deng, Q. Wang, *Chem. Mater.* **2013**, *25*, 2503.
- [162] S. Wilhelm, A. J. Tavares, Q. Dai, S. Ohta, J. Audet, H. F. Dvorak, W. C. W. Chan, **2016**, *1*, 16014.
- [163] D. W. Deng, Y. Q. Chen, J. Cao, J. M. Tian, Z. Y. Qian, S. Achilefu, Y. Q. Gu, *Chem. Mater.* **2012**, *24*, 3029.
- [164] K. T. Yong, I. Roy, R. Hu, H. Ding, H. X. Cai, J. Zhu, X. H. Zhang, E. J. Bergey, P. N. Prasad, *Integr. Biol.* **2010**, *2*, 121.
- [165] L. J. Tan, S. P. Liu, X. Q. Li, I. S. Chronakis, Y. M. Shen, *Colloids Surf. B* **2015**, *125*, 222.
- [166] J. H. Gao, K. Chen, R. G. Xie, J. Xie, S. Lee, Z. Cheng, X. G. Peng, X. Y. Chen, *Small* **2010**, *6*, 256.
- [167] T. Deng, Y. Peng, R. Zhang, J. Wang, J. Zhang, Y. Gu, D. Huang, D. Deng, *ACS Appl. Mater. Interfaces* **2017**, *9*, 11405.
- [168] C. Y. Li, Y. J. Zhang, G. C. Chen, F. Hu, K. Zhao, Q. B. Wang, *Adv. Mater.* **2017**, *29*, 1605754.
- [169] R. Tang, J. Xue, B. Xu, D. Shen, G. P. Sudlow, S. Achilefu, *ACS Nano* **2015**, *9*, 220.
- [170] W. S. Guo, X. L. Sun, O. Jacobson, X. F. Yan, K. Min, A. Srivatsan, G. Niu, D. O. Kiesewetter, J. Chang, X. Y. Chen, *ACS Nano* **2015**, *9*, 488.
- [171] E. Cassette, T. Pons, C. Bouet, M. Helle, L. Bezdetsnaya, F. Marchal, B. Dubertret, *Chem. Mater.* **2010**, *22*, 6117.
- [172] K. T. Yong, I. Roy, R. Hu, H. Ding, H. Cai, J. Zhu, X. Zhang, E. J. Bergey, P. N. Prasad, *Integr. Biol.* **2010**, *2*, 121.

- [173] D. R. Larson, W. R. Zipfel, R. M. Williams, S. W. Clark, M. P. Bruchez, F. W. Wise, W. W. Webb, *Science* **2003**, *300*, 1434.
- [174] J. Zhang, R. G. Xie, W. S. Yang, *Chem. Mater.* **2011**, *23*, 3357.
- [175] D. W. Deng, J. Cao, L. Z. Qu, S. Achilefu, Y. Q. Gu, *Phys. Chem. Chem. Phys.* **2013**, *15*, 5078.
- [176] L. Tan, S. Liu, X. Li, I. S. Chronakis, Y. Shen, *Colloids Surf., B* **2015**, *125*, 222.
- [177] L. Yong Taik, K. Sungjee, N. Akira, E. S. Nathan, G. B. Mounji, V. F. John, *Mol. Imaging* **2003**, *2*, 50.
- [178] Q. B. Wang, *Nanomed.—Nanotechnol. Biol. Med.* **2016**, *12*, 464.
- [179] B. L. Wehrenberg, C. Wang, P. Guyot-Sionnest, *J. Phys. Chem. B* **2002**, *106*, 10634.
- [180] L. Bakueva, I. Gorelikov, S. Musikhin, X. S. Zhao, E. H. Sargent, E. Kumacheva, *Adv. Mater.* **2004**, *16*, 926.
- [181] M. T. Harrison, S. V. Kershaw, M. G. Burt, A. Eychmüller, H. Weller, A. L. Rogach, *Mater. Sci. Eng., B* **2000**, *69*, 355.
- [182] J. D. Tuszynski, J. M. Dixon, *Biomedical Applications of Introductory Physics*, John Wiley and Sons, New York **2001**.
- [183] X. Liu, C. Lee, W.-C. Law, D. Zhu, M. Liu, M. Jeon, J. Kim, P. N. Prasad, C. Kim, M. T. Swihart, *Nano Lett.* **2013**, *13*, 4333.
- [184] W. Stummer, U. Pichlmeier, T. Meinel, O. D. Wiestler, F. Zanella, H. J. Reulen, A. L.-G. S. Group, *Lancet Oncol.* **2006**, *7*, 392.
- [185] E. L. Rosenthal, J. M. Warram, E. de Boer, T. K. Chung, M. L. Korb, M. Brandwein-Gensler, T. V. Strong, C. E. Schmalbach, A. B. Morlandt, G. Agarwal, Y. E. Hartman, W. R. Carroll, J. S. Richman, L. K. Clemons, L. M. Nabell, K. R. Zinn, *Clin. Cancer Res.* **2015**, *21*, 3658.
- [186] C. E. Hoogstins, Q. R. Tummers, K. N. Gaarenstroom, C. D. de Kroon, J. B. Trimbos, T. Bosse, V. T. Smit, J. Vuyk, C. J. van de Velde, A. F. Cohen, P. S. Low, J. Burggraaf, A. L. Vahrmeijer, *Clin. Cancer Res.* **2016**, *22*, 2929.
- [187] Y. Pan, J. Yang, Y. N. Fang, J. H. Zheng, R. Song, C. Q. Yi, *J. Mater. Chem., B* **2017**, *5*, 92.
- [188] X. Q. Su, C. Y. Chan, J. Y. Shi, M. K. Tsang, Y. Pan, C. M. Cheng, O. Gerile, M. Yang, *Biosens. Bioelectron.* **2017**, *92*, 489.
- [189] Y. Liu, A. Q. Bauer, W. J. Akers, G. Sudlow, K. Liang, D. Shen, M. Y. Berezin, J. P. Culver, S. Achilefu, *Surgery* **2011**, *149*, 689.
- [190] V. Biju, S. Mundayoor, R. V. Omkumar, A. Anas, M. Ishikawa, *Biotechnol. Adv.* **2010**, *28*, 199.
- [191] F. M. Winnik, D. Maysinger, *Acc. Chem. Res.* **2013**, *46*, 672.
- [192] N. Chen, Y. He, Y. Su, X. Li, Q. Huang, H. Wang, X. Zhang, R. Tai, C. Fan, *Biomaterials* **2012**, *33*, 1238.
- [193] M. A. Zoroddu, S. Medici, A. Ledda, V. M. Nurchi, J. I. Lachowicz, M. Peana, *Curr. Med. Chem.* **2014**, *21*, 3837.
- [194] N. Kosaka, M. Ogawa, P. L. Choyke, H. Kobayashi, *Future Oncol.* **2009**, *5*, 1501.
- [195] Y. Nakamura, A. Mochida, P. L. Choyke, H. Kobayashi, *Bioconjugate Chem.* **2016**, *27*, 2225.
- [196] J. V. Frangioni, *J. Clin. Oncol.* **2008**, *26*, 4012.
- [197] S. Jeong, I. Song, W. Lee, Y. M. Ryu, Y. Jung, S. Y. Kim, K. Kim, S. C. Hong, S. J. Myung, S. Kim, *Nano Lett.* **2017**, *17*, 1378.
- [198] M. X. Zhao, B. J. Zhu, *Nanoscale Res. Lett.* **2016**, *11*, 207.
- [199] E. Yaghini, A. M. Seifalian, A. J. MacRobert, *Nanomedicine* **2009**, *4*, 353.